AERODYNAMIC INVESTIGATION OF AN AIR-COOLED AXIAL-FLOW TURBINE. PART I. TURBINE DESIGN AND OVERALL STAGE PERFORMANCE WITHOUT SUPPLY OF COOLING AIR

A. Yamamoto, K. Takahara, H. Nouse, S. Inoue,
H. Usui, and F. Mimura

Translation of "Kūrei jikuryū tābin no kūriki seinō ni kan-suru kenkyū. Dai-ippō. Kūrei tābin no sekkei oyobi reikyaku kūki wo nagasanai baai no zentai seinō ni kan-suru jikkenteki kenkyū," National Aerospace Lab., Tokyo (Japan), NAL-TR-321-Pt-1, 1973, 34 pp

NATIONAL AERONAUTICS AND SPACE ADMINISTRATION
WASHINGTON, D.C. 20546 DECEMBER 1974

STANDARD TITLE PAGE

1. Report No. NASA TT F-16,083	2. Government Accession No.	3. Recipient's Catalog No.
4. Title and Subtitle AERODYNAMIC INVESTIGATION OF AN AIR-COOLED AXIAL-FLOW TURBINE. PART I. TURBINE DESIGN AND OVERALL STAGE PERFORMANCE WITHOUT SUPPLY OF COOLING AIR		5. Report Date December 1974 6. Performing Organization Code
7. Author(s) A. Yamamoto, K. Takahara, H. Nouse, S. Inoue, H. Usui, and F. Mimura, Prime Mover Department		8. Performing Organization Report No. 10. Work Unit No.
9. Performing Organization Name and Address Leo Kanner Associates Redwood City, California 94063		11. Contract or Grant No. NASw-2481 13. Type of Report and Period Covered Translation
12. Sponsoring Agency Name and Address National Aeronautics and Space Administration, Washington, D.C. 20546		14. Sponsoring Agency Code

15. Supplementary Notes

Translation of "Kūrei jikuryū tābin no kūriki seinō ni kan-suru kenkyū. Dai-ippō. Kūrei tābin no sekkei oyobi reikyaku kūki wo nagasanai baai no zentai seinō ni kan-suru jikkenteki kenkyū," National Aerospace Lab., Tokyo, (Japan), NAL-TR-321-Pt-1, 1973, 34 pp.

16. Abstract A single-stage turbine with a 22 inch diameter was designed to investigate air-cooled turbines operating in a high-temperature environment. The stator and rotor blades are characterized by low blade solidity, thick blade section, blunt leading edge and trailing edge, and low blade aspect ratio. The turbine satisfied the equivalent design value of specific work output at the design condition with an efficiency of 85.6%. It is concluded that the present airfoil shapes designed for an air-cooled turbine are satisfactory from an aerodynamic standpoint and that changes in the airfoil shape for cooling considerations did not noticeably impair the turbine overall performance.

17. Key Words (Selected by Author(s))	18. Distribution Statement
	Unclassified-Unlimited

19. Security Classif. (of this report)	20. Security Classif. (of this page)	21. No. of Pages	22. Price
Unclassified	Unclassified	69	

TABLE OF CONTENTS

Symbols

A	Area
A_a	Annular area
a	Sound velocity
B_L, B_T	Leading and trailing edge angles of blade
C	Chord length
C_p, C_{pi}	Pressure coefficients of compressible and incompressible fluids
c_p	Specific heat at constant pressure
D_p, D_s, D_t	Blade diffusion parameters
d	Diameter
d_L, d_T	Leading and trailing edge diameters of blade
$d\theta$	Angle
G	Turbine weight flow rate
g	Gravity acceleration
H	Enthalpy
ΔH_T	Turbine thermal head
h	Blade height
i	Blade incidence, also indicates i-th circle
J	Work equivalent of heat; 426.9 kg·m/kcal
L	Specific blade loss; $(1 - \eta_t)/\sigma_M$
ℓ	Arm length of dynamometer; 1.4606 m
M	Mach number
m	$\sin^2\alpha_2$
N	Turbine revolution speed
n	Number of blades
O	Blade throat width
P	Pressure
R	Gas constant
$\overline{R}_e$	Mean Reynolds number inside turbine
R_L, R_T	Leading and trailing edge radii of blade
RF	Temperature recovery coefficient
r	Blade radius in height direction
S	Entropy

S	Blade pitch
T	Temperature
U	Peripheral velocity
V	Absolute velocity
W	Relative velocity
W_T	Dynamometer load
X, Y	Coordinates
Y_t	Total pressure loss coefficient of blade
x	Length (mainly in axial direction)
y	Length (mainly in blade height direction)
z	Length

(Greek letters)

α	Absolute outflow angle
β	Relative outflow angle
γ	Specific weight
δ	Ratio of turbine inlet total pressure to standard pressure
ε, ε_{cr}	Compensation coefficients for flow rate
η	Efficiency
η_T	Adiabatic efficiency based on enthalpy when designing the turbine
η_t	Adiabatic efficiency based on dynamometer output and turbine expansion ratio
η_{1-3}	Adiabatic temperature efficiency based on total temperature ratio and total pressure ratio
θ	Angle
θ, θ_{cr}	Velocity ratio
κ	Specific heat ratio
λ	Air fuel ratio
μ	Coefficient of viscosity
ξ	Angle of stagger
π_T	Turbine expansion ratio
ρ	Density
ρ_R	Degree of reaction
σ	Solidity; C/S
τ	Turbine torque

ϕ, ϕ_{cr}	Compensation coefficients for turbine expansion ratio
φ_N	Velocity coefficient of stator blade
φ_N'	Total pressure ratio before and after stator blade
ϕ	Entropy function
ω	Angular velocity

(Subscripts)

a	Axial direction
ad	Adiabatic
air	Air
cr	Value at M = 1.0
des	Design
i	Incompressible, or i-th
M	Mean (mean diameter)
max	Maximum
N	Stator blade
R	Rotor blade
r	Relative
rad	Radial direction
s	Static
st	Standard state
T	Turbine
t	Total
th	Theoretical
u	Peripheral velocity or peripheral direction
1	Before stator blade
2	After stator blade, before rotor blade
3	After rotor blade
∞	Infinite
$\bar{}$	Mean

AERODYNAMIC INVESTIGATION OF AN AIR-COOLED AXIAL-FLOW TURBINE. PART I. TURBINE DESIGN AND OVERALL STAGE PERFORMANCE WITHOUT SUPPLY OF COOLING AIR

Atsumasa Yamamoto, Kitao Takahara, Hiroyuki Nouse, Siegeo Inoue, Hirosi Usui, and Fujio Mimura

I. Introduction

In recent aircraft there has been a demand for the development of engines with a decreased fuel flow rate by increasing the minimum cycle temperature, improving the thermal efficiency, and using fan engines with an improved propulsive efficiency. It is necessary to cool the turbine blades so that they can withstand this high gas temperature at the turbine inlet. In the aircraft turbines all over the world today, the air coming from the compressor is used to cool the blades, and the turbine inlet temperature has been raised rapidly year by year thanks to progress and improvements in the cooling methods. /3*

In turbines using air-cooled blades, that is, in air-cooled turbines, higher turbine inlet temperatures and higher cycle pressure ratios are dealt with than is the case in non-cooled turbines. For this reason, the blades are required to have various special properties. The most important ones are the following. (1) Since it is necessary to introduce cooling air inside the blades, the leading and trailing edges of the blades will be thicker, and the blades as a whole will be thick. (2) At the higher cycle temperatures, the optimum thermodynamic expansion ratio will increase. Therefore, in order to eliminate as for as possible the necessity for cooling after the second stage, it is necessary to increase the work per stage. The deflection angles in the stator and rotor blades are increased in order for this to be digested by the thick turbine blades. (3) In most cases, the cooling air used for

* Numbers in the margin indicate pagination in the foreign text.

cooling the turbine blades is extracted from the intermediate or final stages of the compressor. For this reason, the increased amount of cooling air will increase the total loss of the engine as a whole, and therefore the necessary amount of cooling air must be suppressed to the utmost minimum [1]. It is necessary to reduce the number of cooling blades for this purpose. (4) Together with the increase in the turbine inlet pressure, the high-pressure turbine blades will become smaller in size, and there will be a relative increase in the decline of the aerodynamic performance on account of the rotor blade tip clearance. (5) Not a very large twisting angle can be obtained in the blades on account of problems connected with fabrication of the cooling holes, etc. (6) On account of escape and leakage of the cooling air from the blades or the inner and outer walls, there occurs aerodynamical interference between the cooling air and the main flow gas, and the aerodynamical performance of the turbine is affected.

Thus, air-cooled blades, which are required to fulfill conditions which are quite different from those of the non-cooled blades, must incorporate more compromises in the design than was the case in the conventional non-cooled blades of the past, and there are also many difficult points in the production. There have been a number of studies overseas concerning turbines with such air-cooled blades [2-4], and their performance properties have been investigated. Nevertheless, the various design problems caused by the foregoing circumstances and the characteristics of the blades have not been clarified to any great degree, and the designing methods themselves have not been established.

In view of these circumstances, our Prime Mover Department is making studies of high-temperature air-cooled turbines as part of its aeronautical engine research. In this report we discuss the designing methods and the results of experiments concerning the aerodynamic performance properties of the early

air-cooled turbines. We first set up the fundamental policies which are necessary in air-cooled turbines and describe a method of designing under these policies in which the conventional designing methods of the past will be applied as far as possible. Next we describe the results of experimental studies to determine whether air-cooled turbines designed in this way display the anticipated aerodynamical overall performance properties or not. Furthermore, some of the problems at issue in this designing method are pointed out on the basis of the results of measurements of the internal flow.

These experiments were conducted using unheated compressed air with a turbine inlet temperature of about 100°C. The experiments were performed without supplying air for cooling the blades.

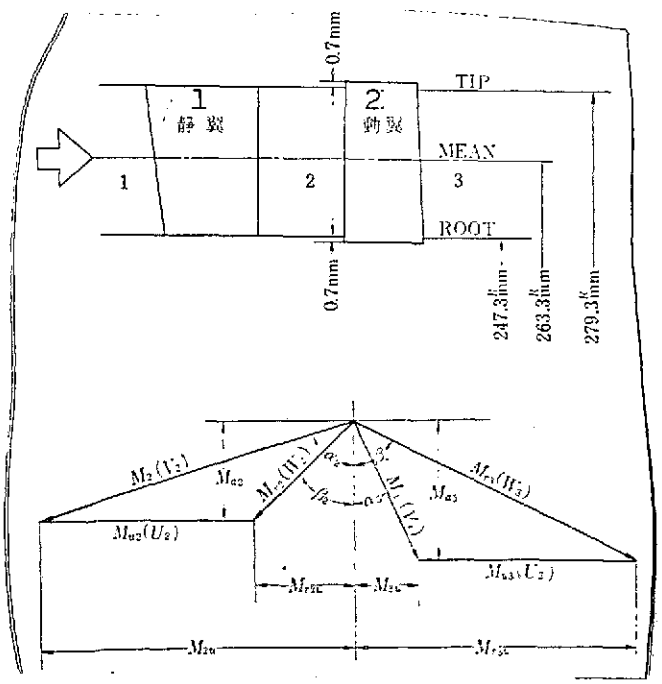

Fig. 1. Inspection sections for design calculations and velocity triangle symbols.

Key: 1. Stator blade
2. Rotor blade

2. Design

/4

At the early stage of research into high-temperature turbines in the Prime Mover Department of this Laboratory, the planning called for a turbine inlet gas temperature of 1,150°C. This turbine had a single stage, and the internal air-cooling system was adopted in both the stator and the rotor blades.

As for the sequence of the aerodynamical designing, we first carried out performance calculations one-dimensionally

for several types of velocity triangles at the mean blade diameter; then the optimum on was selected from them. Next, we performed two-dimensional calculations under the assumption that the performance will be realized by the mean blade diameter (MEAN) and determined the velocity triangle at the blade tip (TIP), the mean blade diameter (MEAN), and blade (ROOT). Finally, the profile and the blade arrangement were determined on the basis of this velocity triangle. In Fig. 1 are shown the inspection section radius and velocity triangle symbols for design calculations. In the designing at this time the flow of cooling air was not taken into consideration in calculation of the gas flow inside the turbine. In the following, an outline is given of this designing. /4*

2.1. Calculation of Turbine Performance

Turbine performance calculations were performed for various turbine revolution speeds, stator blade outflow angles, and stator blade outflow Mach numbers, and those with great turbine work and adiabatic efficiency were selected.

TABLE 1. CHIEF DESIGN SPECIFICATIONS

項目	記号	設計値	単位
ガス流量	G	3.95	kg/sec
入口全圧	P_{t1}	25000	kg/m²
入口全温	T_{t1}	1423.15	°K
断熱効率	η_T	0.85	
断熱熱落差	$\triangle H_{ad}$	63.25	kcal/kg
回転数	N	13300	rpm
周速度	U_M	366.7	m/sec
膨脹比	π_T	2.02	
理論速度	V_{th}	727.5	m/sec
速度比	U_M/V_{th}	0.504	
反動度	$\rho_{R,M}$	0.464	

(Key for table 1 on next page)

Key for Table 1.

1. Item
2. Symbol
3. Design value
4. Unit
5. Gas flow rate
6. Inlet total pressure
7. Inlet total temperature
8. Adiabatic efficiency
9. Adiabatic thermal head
10. Revolution speed
11. Peripheral velocity
12. Expansion ratio
13. Theoretical vlocity
14. Velocity ratio
15. Degree of reaction

The design hypotheses are as follows.

(1) It is assumed that the state of the air current in the inspection sections is uniform in each section, and the state of the air current is calculated one-dimensionally as an adiabatic flow of a perfect gas at the mean blade diameter.

(2) The stator blade velocity coefficient is assumed to be $\phi_N = 0.97$.

(3) The rotor blade total pressure loss coefficient is assumed to be $Y_{tR} = 0.23$.

(4) The specific heat ratio is assumed to be constant i /5 inside the turbine. The specific heat ratio corresponding to the mean temperature of the turbine inlet and outlet temperatures is taken and calculated as $\kappa = 1.315$.

(5) The effects of the cooling air on the main current flow are ignored, and the amount of loss is taken into consideration later on when calculating the turbine adiabatic efficiency.

In Table 1 are shown the results of calculations obtained under the above hypotheses (for details refer to Appendix A.1.).

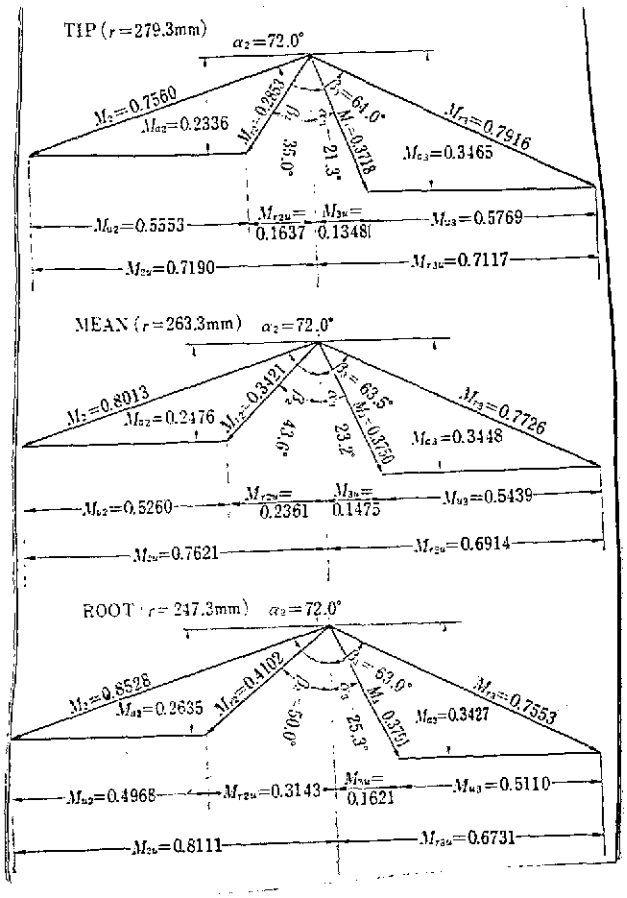

Fig. 2. Design velocity triangles

2.2. Calculation of the Velocity Triangles

On the basis of the several hypotheses given below, more detailed calculations were performed at the TIP, the MEAN, and the ROOT, based on the cycle values at MEAN determined in section 2.1, and the velocity triangles at each position were determined. In making these calculations, it was assumed that the stator blade outflow angle was constant in the radial direction. This is so because when such blades are adopted the stator blades will have almost a constant section in the blade height direction, and fabrication of the internal cooling holes will be easy. Consequently, such blades are suitable for air-cooled blades.

The design hypotheses are as follows:

Hypotheses concerning the streamlines:

(1) The flow inside the turbine is constant. It is also /6 an adiabatic flow and is treated as a perfect gas.

(2) The streamlines are parallel to the rotor blade axis, and the velocity components in the radial direction are ignored in each inspection section.

Hypotheses concerning the stator blades:

(3) The total temperature and total pressure at the stator blade inlet are constant in the radial direction.

TABLE 2((a). RESULTS OF CALCULATIONS OF STATOR BLADE PROFILE AN AND BLADE ARRANGEMENTS (TIP; r=277.3 mm)

BLADE PROFILE NOZZLE (TIP)

C	ξ	B_L	B_T
33.600	−45.000	6.000	−71.000

BLADE COORDINATES

	ORIGINAL		CAMBER LINE		BLADE SURFACE			
	(X^*, Y^*)		$CAM\ (X, Y)$		$S.S\ (X, Y)$		$P.S\ (X, Y)$	
i	X	Y	X	Y	X	Y	X	Y
1	1.456	2.218	2.213	0.154	2.152	2.371	2.273	− 2.063
2	2.463	2.860	3.628	0.144	3.754	3.002	3.501	− 2.713
3	3.655	3.210	5.172	0.003	5.623	3.182	4.722	− 3.175
4	4.878	3.356	6.620	0.279	7.438	2.976	5.801	− 3.534
5	6.314	3.619	8.160	− 0.769	9.469	2.605	6.851	− 4.143
6	7.902	3.677	9.694	− 1.481	11.450	1.750	7.937	− 4.711
7	9.825	3.488	11.355	− 2.540	13.420	0.270	9.290	− 5.350
8	11.872	3.239	12.933	− 3.857	15.150	− 1.495	10.716	− 6.219
9	14.056	3.020	14.444	− 5.434	16.725	− 3.455	12.162	− 7.414
10	16.483	2.597	15.957	− 7.354	18.064	− 5.835	13.850	− 8.873
11	18.882	2.276	17.314	− 9.389	19.249	− 8.191	15.379	−10.588
12	21.510	1.999	18.673	−11.746	20.433	−10.798	16.913	−12.694
13	24.241	1.693	19.970	−14.312	21.499	−13.585	18.442	−15.039
14	27.113	1.343	21.228	−17.115	22.464	−16.590	19.992	−17.640
15	30.199	0.948	22.480	−20.228	23.366	−19.890	21.594	−20.566
16	33.147	0.525	23.594	−23.283	24.090	−23.110	23.098	−23.456

CAMEER LINE $a_3=-0.00142$ $a_2=-0.01288$ $a_1=0.10510$

n	S	S/C	THROAT POSITION				THROAT LENGTH O	ARCCOS O/S
			$P.S\ (X, Y)$		$S.S\ (X, Y)$			
71	24.540	0.730	23.098	−23.456	16.459	−27.548	7.798	71.471
72	24.199	0.720	23.098	−23.456	16.593	−27.414	7.615	71.659
73	23.868	0.710	23.098	−23.456	16.715	−27.293	7.448	71.818
74	23.545	0.701	23.098	−23.456	16.835	−27.174	7.284	71.980
75	23.231	0.691	23.098	−23.456	16.965	−27.054	7.111	72.175

(4) The total pressure loss of the stator blades is constant in the radial direction.

(5) The absolute outflow angle of the stator blade is constant in the radial direction.

(6) At the stator blade outlet, the flow satisfies the conditional equation for simple radial balance.

Hypotheses concerning the rotor blades:

TABLE 2 (b). RESULTS OF CALCULATIONS OF STATOR BLADE PROFILE AND BLADE ARRANGEMENT (MEAN; r=261.3 mm)

表 2 (b) 静翼の翼型および翼配備の計算結果 (MEAN; r=261.3 mm)

BLADE PROFILE NOZZLE (MEAN)

C	ξ	B_L	B_T
31.700	−45.000	8.000	−71.000

BLADE COORDINATES

	ORIGINAL		CAMBER LINE		BLADE SURFACE			
	(X^*, Y^*)		$CAM\ (Y, X)$		$S.S\ (X, Y)$		$P.S\ (X, Y)$	
i	X	Y	X	Y	X	Y	X	X
1	1.326	2.092	2.082	0.206	1.976	2.295	2.188	− 1.883
2	2.279	2.698	3.445	0.222	3.524	2.919	3.366	− 2.474
3	3.405	3.028	4.919	0.104	5.324	3.104	4.513	− 2.897
4	4.561	3.166	6.290	− 0.159	7.062	2.911	5.518	− 3.230
5	5.917	3.413	7.743	− 0.625	8.992	2.551	6.494	− 3.802
6	7.417	3.468	9.185	− 1.305	10.863	1.730	7.506	− 4.340
7	9.235	3.269	10.744	− 2.316	12.713	0.319	8.775	− 4.951
8	11.169	3.055	12.225	− 3.571	14.331	− 1.358	10.118	− 5.784
9	13.233	2.849	13.643	− 5.071	15.806	− 3.217	11.479	− 6.925
10	15.526	2.450	15.064	− 6.894	17.058	− 5.470	13.070	− 8.317
11	17.793	2.147	16.340	− 8.824	18.169	− 7.699	14.511	− 9.948
12	20.276	1.886	17.619	−11.056	19.281	−10.165	15.957	−11.946
13	22.857	1.597	18.840	−13.485	20.283	−12.801	17.397	−14.168
14	25.570	1.266	20.026	−16.135	21.192	−15.642	18.860	−16.629
15	28.487	0.895	21.208	−19.079	22.043	−18.760	20.372	−19.397
16	31.272	0.495	22.359	−21.966	22.727	−21.802	21.792	−22.129

CAMBER LINE $a_2=-0.00152$ $a_5=-0.01681$ $a_1=0.14054$

n	S	S/C	THROAT POSITION				THROAT LENGTH O	ARCCOS O/S
			$P.S\ (X, Y)$		$S.S\ (X, Y)$			
⑦1	23.124	0.729	21.792	−22.129	15.551	−25.922	7.303	71.589
72	22.803	0.719	21.792	−22.129	15.680	−25.795	7.127	71.788
73	22.490	0.709	21.792	−22.129	15.793	−25.685	6.974	71.937
74	22.186	0.700	21.792	−22.129	15.904	−25.577	6.823	72.088
75	21.891	0.691	21.792	−22.129	16.022	−25.470	6.667	72.268

(7) The distribution of the rotor blade work (thermal head) is constant in the radial direction.

(8) The rotor blade adiabatic efficiency is constant in the radial direction.

(9) At the rotor blade outlet, the flow satisfies the conditional equation for simple radial balance.

In Fig. 2 are shown the results of calculations obtained under the above hypotheses (for details refer to Appendix A.2).

2.3. Determining the Profile and the Blade Arrangement of Air-Cooled Blades

TABLE 2 (c). RESULTS OF CALCULATIONS OF STATOR BLADE PROFILE AND BLADE ARRANGEMENTS (ROOT; r=245.3 mm)

BLADE PROFILE NOZZLE (ROOT)

C	ξ	B_L	B_T
29.800	−45.000	8.000	−71.000

BLADE COORDINATES

	ORIGINAL		CAMBER LINE		BLADE SURFACE			
	(X^*, Y^*)		$CAM\,(X, Y)$		$S.S\,(X, Y)$		$P.S\,(X, Y)$	
i	X	Y	X	Y	X	Y	X	Y
1	1.247	1.967	1.957	0.194	1.858	2.158	2.057	− 1.771
2	2.142	2.536	3.239	0.209	3.314	2.744	3.164	− 2.326
3	3.201	2.847	4.624	0.097	5.005	2.919	4.243	− 2.724
4	4.287	2.976	5.913	− 0.150	6.639	2.737	5.188	− 3.037
5	5.563	3.209	7.279	− 0.588	8.453	2.399	6.104	− 3.575
6	6.973	3.261	8.634	− 1.227	10.212	1.627	7.056	− 4.081
7	8.682	3.093	10.100	− 2.177	11.952	0.300	8.249	− 4.655
8	10.500	2.873	11.492	− 3.357	13.473	− 1.277	9.511	− 5.438
9	12.440	2.679	12.825	− 4.768	14.859	− 3.024	10.791	− 6.511
10	14.596	2.304	14.161	− 6.481	16.036	− 5.142	12.286	− 7.819
11	16.727	2.019	15.361	− 8.295	17.081	− 7.238	13.641	− 9.352
12	19.061	1.773	16.563	−10.393	18.126	− 9.556	15.000	−11.230
13	21.488	1.501	17.711	−12.677	19.068	−12.034	16.355	−13.319
14	24.038	1.191	18.826	−15.169	19.922	−14.704	17.730	−15.633
15	26.780	0.841	19.937	−17.936	20.723	−17.636	19.151	−18.235
16	29.398	0.466	20.925	−20.649	21.365	−20.496	20.486	−20.803

CAMBER LINE a_3=−0.00172 a_2=−0.01789 a_1=0.14054

n	S	S/C	THROAT POSITION				THROAT LENGTH O	ARCCOS O/S
			$P.S\,(X, Y)$		$S.S\,(X, Y)$			
㉑	21.708	0.728	20.486	−20.803	14.628	−24.358	6.852	71.600
72	21.406	0.718	20.486	−20.803	14.738	−24.247	6.701	71.759
73	21.113	0.708	20.486	−20.803	14.851	−24.139	6.548	71.932
74	20.828	0.699	20.486	−20.803	14.974	−24.026	6.385	72.147
75	20.550	0.690	20.486	−20.803	15.070	−23.935	6.256	72.275

Since the blades are air-cooled blades, in determining /7 the profiles for both the stator blades and the rotor blades, the following items were taken as the fundamental policies (for details refer to Appendix A.3).

(1) The aforementioned velocity triangle shall be satisfied.

(2) The number of blades shall be decreased as far as possible so that it will be possible to do with the minimum necessary amount of cooling air.

(3) Since cooling air is passed through the interior of the blades, the leading and trailing edges of the blades will be made thicker than in ordinary non-cooled blades in view of the fabrication of the cooling holes.

(4) The leading and trailing edges of the blades at each section shall be passed through in a straight line with respect to the blade span direction on account of the fabrication of the cooling holes.

(5) The cooled blades shall have a construction in which there will be a low external heat transfer ratio and a high internal heat transfer ratio.

In Table 2 (a) - (c) are shown the results of calculations of the stator blade profiles and blade arrangements obtained under the above fundamental policies. These results for the profiles and blade arrangements were plotted with an X-Y plotter, and an example of this (MEAN) is shown in Fig. 3. The chief dimensions of the blades are organized in Table 3. Here, since during manufacturing of the blades the leading edge diameter of the blades (d_T) and the trailing edge thickness (d_L) were finally assumed to be constant in the blade span direction and were given values of 4 mm and 2 mm, respectively, they differ slightly from the computer results shown in Table 5.

The coordinates of the rotor blade profiles and blade arrangements are shown in Table 4, and the chief dimensions of the blades are shown in Table 5.

The arrangements of the stator and rotor blades at the mean blade diameters are shown in Fig. 4.

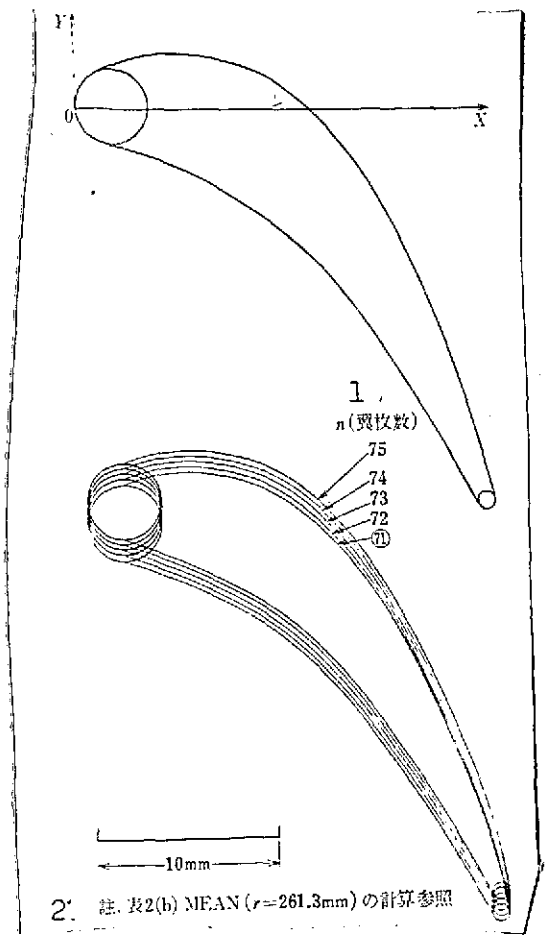

Fig. 3. Stator blade arrangements by X-Y plotter (MEAN)
Key:
1. n (number of blades)
2. Note: Refer to Table 2 (b), calculations of MEAN (r = 261.3 mm)

3. Experiments

3.1. Experimental Equipment and Measuring Equipment

An outline of the experimental equipment is shown in Fig. 5.

The measuring equipment is as follows.

The turbine air flow rate /10 was measured by means of the JIS standard disk type orifice.

The turbine axial torque was measured by means of an automatic Ward-Leonard type 1,600 kW D.C. electric dynamometer. The turbine revolution speed was measured by means of the magnetic pulses from the reduction gear (reduction ratio 1:12.984) mounted on the dynamometer axis.

The gaseous states were measured before and after the turbine. The gas temperature was measured by means of a CA thermocouple thermometer [5, 6], and the total pressure, static pressure, Mach number, and angles were measured by means of three-hole yaw meters[7]. The sensors for measuring these gaseous states were fastened before the turbine at definite positions, and after the turbine they were arranged so that they would be able to traverse in the radial direction.

The types of these measuring instruments and the measuring

positions are shown in Table 6 and Fig. 6. Photographs of the main parts of the measuring instruments and of the driving part of the motor-driven traversing device are shown in Fig. 7.

TABLE 3. CHIEF DIMENSIONS OF STATOR BLADES

n=71 翼 1		TIP (r=277.3 mm)	MEAN (r=261.3 mm)	ROOT (r=245.3 mm)	注 1 2
d_L*	(mm)	4.00	4.00	4.00	注 2 3
d_L (X, Y)	(mm)	(2.21, 0.15)	(2.08, 0.21)	(1.96, 0.19)	
d_T*	(mm)	1.00	1.00	1.00	注 3 4
d_T (X, Y)	(mm)	(23.59, -23.28)	(22.26, -21.97)	(20.93, -20.65)	
d_{max}*	(mm)	7.36	6.94	6.52	
d_{max} (X, Y)	(mm)	(9.69, -1.48)	(9.19, -1.31)	(8.63, -1.23)	
C	(mm)	33.60	31.70	29.80	
S	(mm)	24.540	23.124	21.708	
O	(mm)	7.798	7.303	6.852	
B_L	(deg.)	6.00	8.09	8.00	
B_T	(deg.)	71.00	71.00	71.00	
ξ	(deg.)	45.00	45.00	45.00	

5 注 1 * 印は速度三角形の計算時より，各々 2 mm ずつ小さい．(図 1 参照)
6 注 2 〃 印の値（計算時の値は表 2 の i=1 参照)
7 注 3 〃 （ 〃 i=16 〃)

Key:

1. n=71 blades
2. Note 1
3. Note 2
4. Note 3
5. Note 1. r is 2 mm less than when the velocity triangles were calculated
6. Note 2. Value during manufacturing (for the values during calculation refer to i=1 in Table 2)
7. Note 3. Value during manufacturing (for values during calculation refer to i=16 in Table 2).

The measuring and processing system used in the experiments is shown in Fig. 8 [8]. These experiments were planned so that it would be possible to use computers to make the measurements and record the results automatically within a short time. /11

TABLE 4. COORDINATES OF ROTOR BLADE PROFILE AND BLADE ARRANGEMENTS

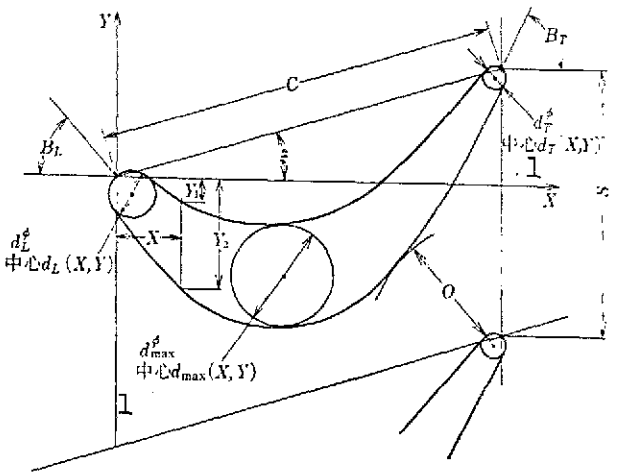

	TIP (r=279.3 mm)		MEAN (r=263.3 mm)		ROOT (r=247.3 mm)	
X (mm)	Y_1 (mm)	Y_2 (mm)	Y_1 (mm)	Y_2 (mm)	Y_1 (mm)	Y_2 (mm)
0.00	0.00	−1.20	0.00	−0.55	0.00	−1.90
1.00	0.33	−2.48	0.20	−3.00	0.08	−3.57
2.00	−0.20	−3.60	−0.49	−4.25	−0.85	−5.00
3.00	−0.67	−4.45	−1.13	−5.25	−1.68	−6.15
4.00	−1.00	−5.07	−1.60	−6.00	−2.30	−6.98
5.00	−1.17	−5.45	−1.95	−6.45	−2.75	−7.60
6.00	−1.23	−5.60	−2.12	−6.75	−3.05	−7.95
7.00	−1.14	−5.53	−2.12	−6.80	−3.22	−8.13
8.00	−0.83	−5.29	−1.98	−6.70	−3.20	−8.15
9.00	−0.35	−4.80	−1.68	−6.40	−3.03	−7.95
10.00	0.29	−4.14	−1.20	−5.93	−2.72	−7.58
11.00	1.05	−3.26	−0.65	−5.20	−2.27	−7.00
12.00	2.00	−2.15	0.13	−4.45	−1.60	−6.15
13.00	3.10	−1.00	1.05	−3.20	−0.75	−5.15
14.00	4.17	0.55	2.13	−1.80	0.22	−3.90
15.00	5.31	2.30	3.25	−0.10	1.25	−2.30
16.00	6.50	4.15	4.45	1.75	2.40	−0.50
17.00	——	6.30	——	3.70	——	1.30

/9

Key:
1
1: Center

TABEE 5. CHIEF DIMENSIONS OF ROTOR BLADES

n=136 枚	1	TIP (r=279.3 mm)	MEAN (r=263.3 mm)	ROOT (r=247.3 mm)
d_L°	(mm)	2.00	2.00	2.00
d_L (X, C)	(mm)	(0.75, -0.65)	(0.65, -0.75)	(0.57, -0.85)
d_T°	(mm)	1.00	1.00	1.00
d_T (X, Y)	(mm)	(16.50, 6.33)	(16.92, 5.75)	(17.35, 3.25)
d_{max}°	(mm)	4.35	4.63	4.92
d_{max} (X, Y)	(mm)	(6.45, -3.45)	(7.3, -4.45)	(7.6, -5.70)
C	(mm)	18.05	18.00	18.00
S	(mm)	12.904	12.164	11.425
O	(mm)	5.75	5.15	4.76
B_L	(deg.)	41.0	49.8	55.8
B_T	(deg.)	64.5	63.5	62.5
ξ	(deg.)	22.5	17.2	11.7

Key:

1. n=136 blades

3.2. Experimental Methods

In these experiments, the turbine expansion ratio and revolution speeds were adjusted to conform with the target values. The expansion ratio of the experimental target was 1.4 - 2.1 with intervals of about 0.2, and the revolution speeds were 70 - 110% of the design value with intervals of about 10%. The measurements were performed by means of two thermometers and two pressure meters at the turbine outlet; traversing measurements were performed in the radial direction. Before these experiments it was ascertained that the temperatures and pressures at the turbine inlet are uniform in the radial direction and in the circumferential direction. /11

In cases when relatively low-temperature air is used, as in these experiments, drops of water are frequently attached to the sensors inserted inside the turbines. In order to

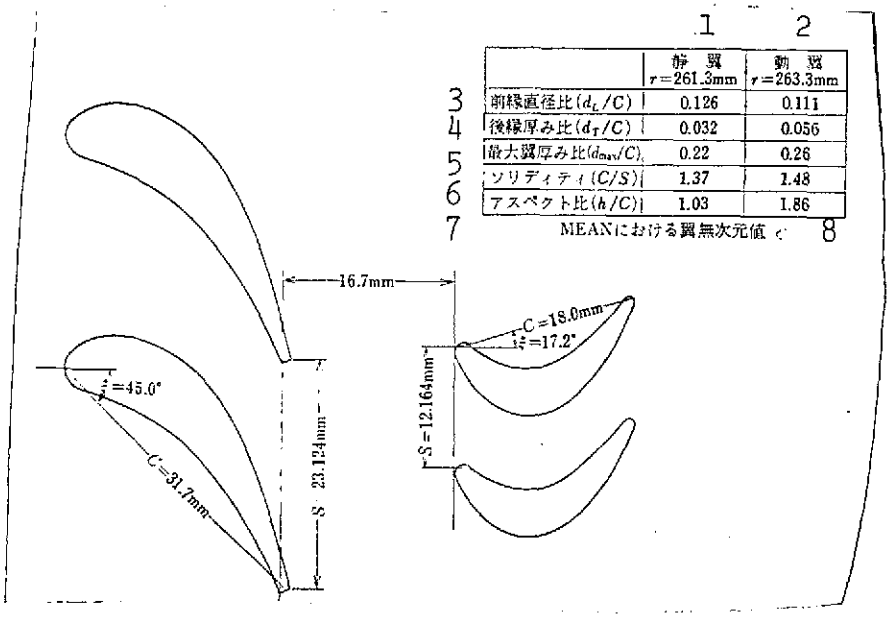

Fig. 4. Stator blades and blade arrangements (MEAN)

Key:

1. Stator blades
2. Rotor blades
3. Leading edge diameter ratio
4. Trailing edge thickness ratio
5. Maximum blade thickness ratio
6. Solidity
7. Aspect ratio
8. Blade dimensionless values at MEAN

prevent this, it was necessary to adjust the turbine expansion ratio and the revolution speed while paying careful attention to make sure that the turbine outlet temperature would not drop below the dew point temperature of that day even once while the experimental points were being set. In this way, traversing measurements were commenced in a state at which the turbine inlet temperature would be more or less stable at about 90-110°C. In cases when traversing measurements were performed at five points, the time required for one experimental point was approximately ten minutes. /11

3.3. Methods of Analyzing the Experiments

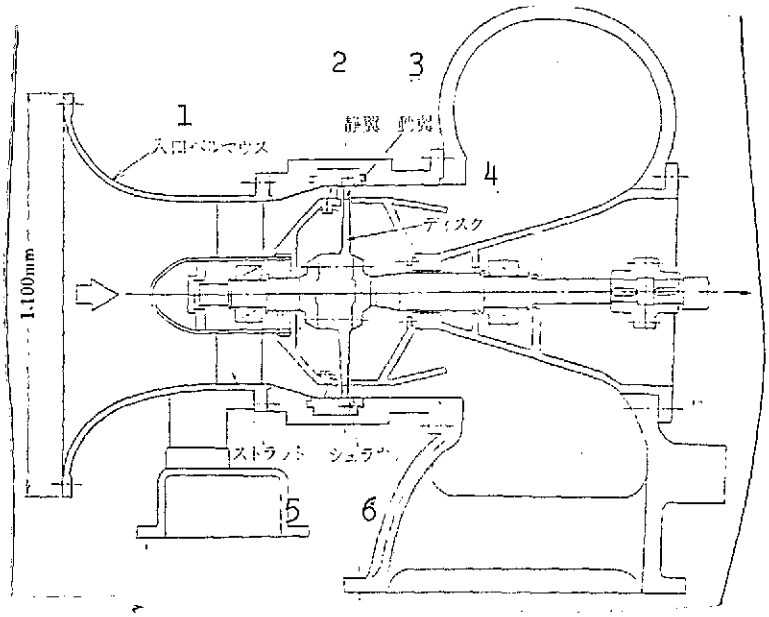

Fig. 5. Main unit of testing device for aerodynamic performance.

Key:
1. Inlet bellmouth
2. Stator blade
3. Rotor blade
4. Disk
5. Strut
6. Shroud

The turbine flow rate G (kg/sec) was calculated by means of the orifice flow rate formula (refer to item 9 in bibliography).

The turbine torque τ (kg·m) was sought by means of the following formula from the dynamometer load W_T (kg) and the arm length of the dynamometer l (m).

$$\tau = l \cdot W_T$$

The turbine specific output ΔH_T (kcal/kg) was calculated by the following formula from the flow rate G (kg/sec), the torque τ (kg·m), and the turbine revolution speed N (rpm).

$$\Delta H_T = \frac{2\pi}{60J} \cdot \frac{\tau \cdot N}{G}$$

The turbine expansion ratio π_T was sought by the following formula as the ratio [illegible].

$$\pi_T = \frac{P_{t1}}{P_{t3}}$$

Here, P_{t1} is the mean total pressure before the stator blade; we used the [illegible] of the total pressure measured at the center of the flow channel [illegible] two Pitot tubes before the stator blade ($3P_{t1}$ - 1 and [illegible]. P_{t3} is the mean total pressure after the rotor blade; [illegible] the radial direction by means of [illegible] two of the Pitot

tubes after the [illegible]. The mathematical mean [illegible] of a total of ten points measured [illegible].

The [illegible] adiabatic efficiency η_T was calculated as one of the adiabatic efficiencies of the turbine.

$$\eta_t = \frac{\Delta H_T}{c_p \cdot T_{t1}\left\{1-\left(\frac{1}{\pi_T}\right)^{\frac{\kappa-1}{\kappa}}\right\}}$$

The following correction values taking into considerations the differences [illegible] design and during experiment [el [illegible] in order to compare [illegible] the above experimental values and the design values . . . . turbine inlet gas state and turbine [illegible] on the basis of the critical velocity calculated from [illegible] is a method of determining approximately the condition [illegible] (Refer to [illegible].

Flow rate G	Corrected flow rate $G\sqrt{\theta_{cr}}/\varepsilon_{cr}\cdot\delta$
Revolution speed N	Corrected revolution speed $N/\sqrt{\theta_{cr}}$
Specific output ΔH_T	Corrected specific output $\Delta H_T/\theta_{cr}$
Torque τ	Corrected torque $\varepsilon_{cr}\cdot\tau/\delta$
Expansion ratio π_T	Corrected expansion ratio $\phi_{cr}\cdot\pi_T$

Here, θ_{cr}, δ, ε_{cr}, and ϕ_{cr} are correction coefficients and are expressed by the following formulas.

$$\theta_{cr} = \left(\frac{\kappa}{\kappa+1}\cdot R\cdot T_{t1}\right)\Big/\left(\frac{\kappa_{st}}{\kappa_{st}+1}R_{st}\cdot T_{t,st}\right)$$

$$\delta = P_{t1}/P_{t,st}$$

$$\varepsilon_{cr} = \left\{\kappa_{st}\left(\frac{\kappa+1}{2}\right)^{\frac{\kappa}{\kappa-1}}\right\}\Big/\left\{\kappa\left(\frac{\kappa_{st}+1}{2}\right)^{\frac{\kappa_{st}}{\kappa_{st}-1}}\right\}$$

$$\phi_{cr} = \frac{1}{\pi_T}\cdot\left\{1-\left(\frac{\kappa_{st}-1}{\kappa_{st}}\right)\left(\frac{\kappa+1}{\kappa-1}\right)\times\left(1-\pi_T^{\frac{\kappa-1}{\kappa}}\right)\right\}^{\frac{\kappa_{st}}{\kappa_{st}-1}}$$

TABLE6. TYPES OF MEASURING DEVICES (REFER TO FIG. 6)

名1称	軸方向計測位置* 2	円周方向計測位置* 3	トラバース方向 4	型式など5
$3P_{t1}$-1	A	3	半径方向 6	5孔ピトー管の内3孔を用いる(7) 8
$3P_{t1}$-2	A	5	〃	〃
P_{w1}-1	B	1	—	外壁静圧タップ
P_{w1}-2	B	6	—	〃 9
T_1-1	B	2	半径方向 6	せき止め型CA熱電対温度計(5)
T_1-2	B	4	〃	(RF=1.0) 10
$3P_{t3}$-1	C	9	〃	5孔ピトー管の内孔を用いる(7),
$3P_{t3}$-2	C	11	〃	〃 11
P_{w3}-1	D	7	—	外壁静圧タップ,
P_{w3}-2	D	12	—	〃 12
T_3-1	D	8	半径方向 6	先端露出型CA熱電対温度計
T_3-2	D	10	〃	(RF≒0.7～0.82) 13
$7P_{t3}$-R	E	13	半径方向	円周方向くし型7孔ピート管
$3P_{t3}$-R	F	14	半径，円周方向	3孔ピト－14管

15 * 図6参照 7

/12

Key:

1. Appellations
2. Measuring positions in axial direction*
3. Measuring positions in circumferential direction*
4. Traversing direction
5. Type-form, etc.
6. Radial direction
7. Radial direction
8. Radial, circumferential directions
8. Three holes in a five-hole Pitot tube are used [7]
9. Outer wall static pressure taps
10. Damming type CA thermocouple thermometer [5]
11. Inner holes of a five-hole Pitot tube are used [7]
12. Outer wall static pressure taps
13. Tip exposed type CA thermocouple thermometer
14. Circumferential direction comb type seven-hole Pitot tube, Three-hole Pitot tube
15. * Refer to Fig. 6.

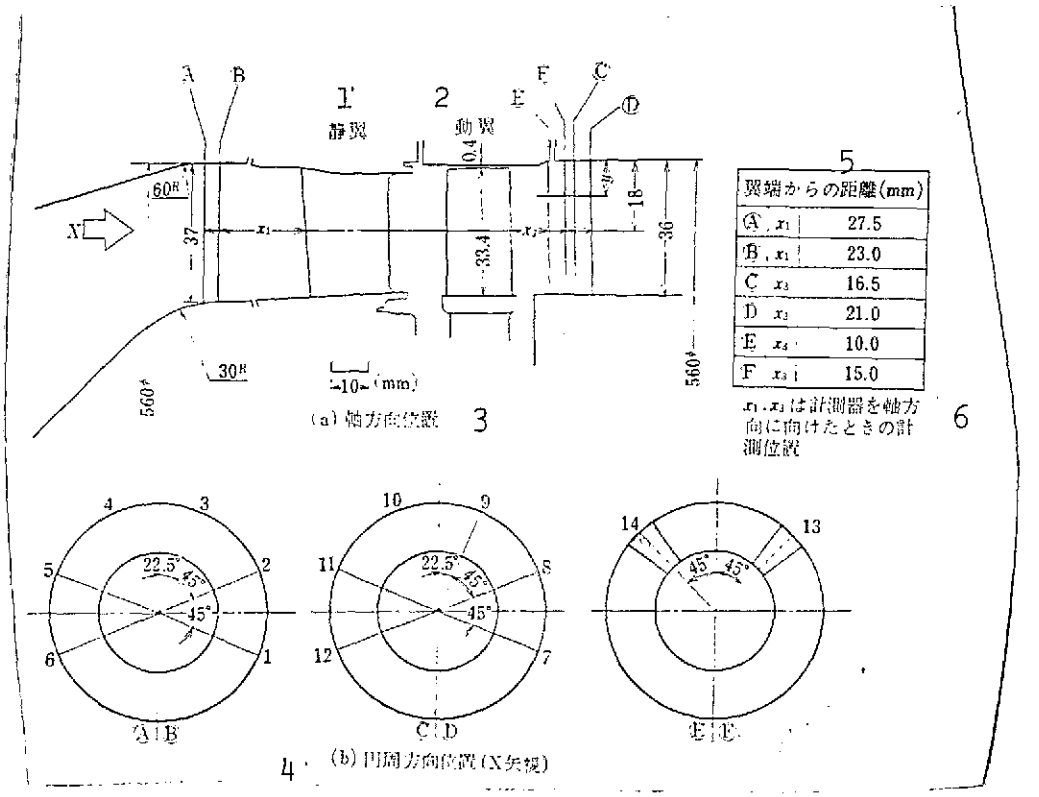

Fig. 6. Measuring positions of various measuring instruments (refer to Table 6)

Key:

1. Stator blade
2. Rotor blade
3. (a) Positions in axial direction
4. (b) Positions in circumferential direction (view at X arrow)
5. Distance from blade end (mm)
6. x_1 and x_3 are measuring positions when measuring instrument is faced in the axial direction

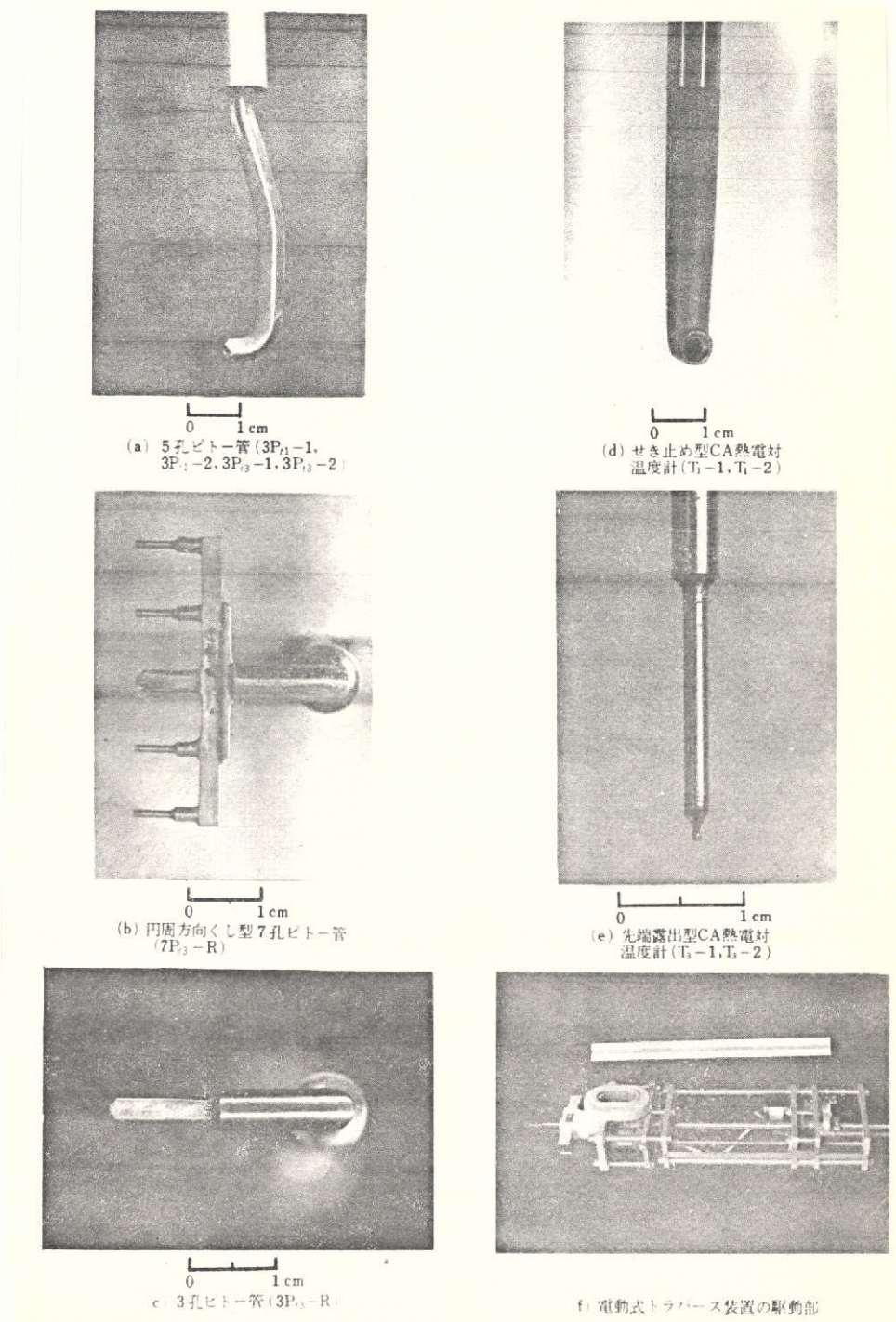

Fig. 7. Photographs of main parts of measuring instruments and of driving parts of motor-driven type traversing device

(Key on following page)

Key for Fig. 7.

(a) Five-hole Pitot tube
(b) Circumferential direction comb type seven-hole Pitot tube
(c) Three-hole Pitot tube
(d) Damming type CA thermocouple thermometer
(e) Tip exposed type CA thermocouple thermometer
(f) Driving parts of motor-driven type traversing device

The suffix st indicates the standard state. The following values were adopted here as the standard values:

$T_{t,st}$= 288.2°K

$P_{t,st}$=110332 kg/m^2

R_{st}= 29.27 kg·m/°K·kg

K_{st}= 1.401

/14

To use these corrected values signifies that the design values and the experimental values will always be corrected to the values at the standard state and compared. In Table 7 are shown the various disign values and their corrected values. In finding these corrected values, it was assumed that the mean specific heat ratio inside the turbine was 1.31 (refer to the value of No. 51 in Appendix Table 2) and that the gas constant was 29.27 kg·m/°K·kg.

3.4. Experimental Results

(a) Flow Rate Characteristics (Fig. 9)

According to Fig. 9, the corrected flow rate is 3.98 kg/sec at the design corrected revolution speed and the design corrected expansion ratio (2.09). The differences in these flow rate curves caused by the revolution speed indicate that the flow rate is governed by the rotor blade. Furthermore, this turbine is choked by the rotor blade, and the expansion ratio at which it is believed that there is choking at all the revolution speeds in the experiment is about 2.3.

(b) Torque Characteristics (Fig. 10)

Concerning the flow rate, it is believed that choking will be caused by a corrected expansion ratio of about 2.3, as was mentioned above. As for the torque, however, a /15 tendency towards increase still continues to be displayed even after this expansion ratio is exceeded. It always increases together with the expansion ratio at all the revolution speeds in the experiment. Thus, in this turbine, there is seen no torque limit (limiting loading) within the range of the experiments. Furthermore, the corrected torque in the experiments is 30.2 kg·m at the design corrected revolution speed and the design corrected expansion ratio. This is a value approximately 8.2% greater than the design value.

(c) Map of Overall Performance (Fig. 11)

In Fig. 11 is shown a map of the overall performance compiled from the flow rate characteristics in Fig. 9 and from the torque characteristics in Fig. 10. Here the corrected specific output $\Delta H_T/\theta_{cr}$ is plotted on the ordinate, and the corrected flow rate revolution speed parameter (corrected flow rate x corrected revolution speed) $G_{cr}\cdot N/\delta$ is plotted on the abscissa. The results are plotted in terms of equal corrected revolution speed lines, equal corrected expansion ratio lines, and equal adiabatic efficiency lines. According to this, the adiabatic efficiency η_t is 0.7 - 0.865 within the range of the experiments. The maximum adiabatic efficiency is obtained in the vicinity of a corrected revolution speed of 90% and of a corrected expansion ratio of 1.72. Its value is 0.865.

The D point, that is, the point of the design corrected revolution speed and the design corrected expansion ratio, was shown by the O mark. The corrected specific output obtained at this time is 11.22 kcal/kg, and the adiabatic efficiency is 0.856.

(d) Absolute Outflow Angle of Rotor Blade (Fig. 12)

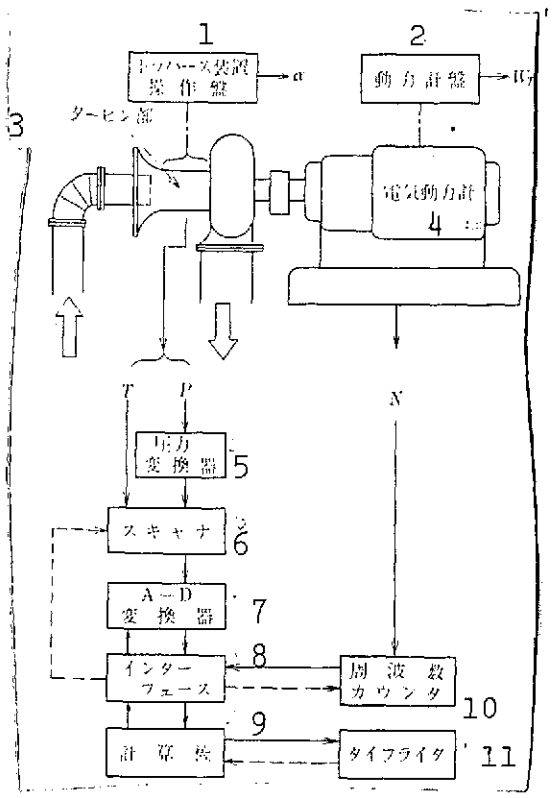

Fig. 8. Measuring-processing system

Key:

1. Control panel of traversing device
2. Dynamometer panel
3. Turbine part
4. Electric dynamometer
5. Pressure converter
6. Scanner
7. A-D converter
8. Interface
9. Computer
10. Frequency counter
11. Typewriter

According to the results /16 of measurements of the absolute outflow angles from the rotor blade by means of the four Pitot tubes installed in the circumferential direction at the rotor blade outlet, there are almost no differences in the measuring angles of the four Pitot tubes at the center of the channel, and it is thought that one may regard the absolute outflow angles in the circumferential direction as being more or less uniform at this position. For this reason, it was decided to select the outflow angle at the center of the channel as the value representing the absolute outflow angles at the rotor blade outlets. It is clear from this figure that the rotor blade absolute outflow angle is 21.5° at the design corrected revolution speed and the design corrected expansion ratio. This is 1.8° smaller than the design value at the mean blade diameter. As will be mentioned below, this is the result of the fact thatthe deflection angle of the rotor blade has decreased.

(e) Rotor Blade Absolute Outflow Mach Number (Fig. 13)

According to the experiments, the absolute outflow Mach number at the rotor blade outlet had a distribution in the

TABLE 7. DESIGN VALUES AND THEIR CORRECTED VALUES (κ_{des}= 1.31)

1 設計項目	2 設計値	3 修正値
4 入口全温 T_{t1} (°k)	1423.2	288.2
5 入口全圧 P_{t1} (kg/m²)	25000	10332
6 比仕事 HT (kcal/kg)	53.8	11.2
7 流量 G (kg/sec)	3.95	3.71
8 回転数 N (rpm)	13300	6071
9 膨脹比 π_T	2.02	2.09

Key:

1. Design items
2. Design values
3. Corrected values
4. Inlet total temperature
5. Inlet total pressure
6. Specific output
7. Flow rate
8. Revolution speed
9. Expansion ratio

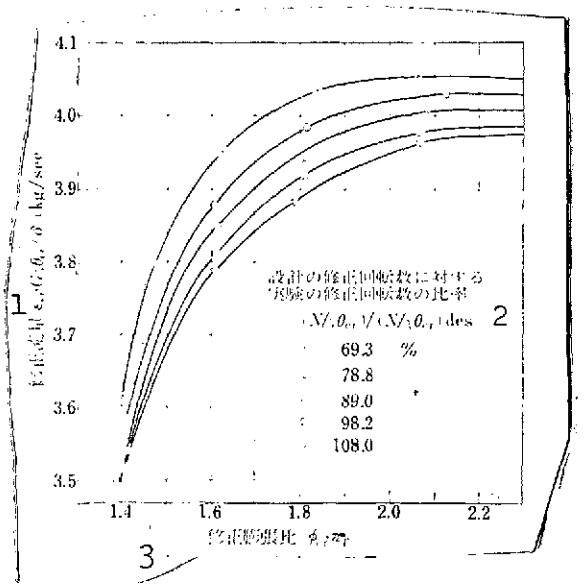

Fig. 9. Flow rate characteristics

radial direction, but at the center of the channel it could be regarded as being more or less uniform in the circumferential direction, just like the rotor blade absolute outflow angle. Here are shown the rotor blade absolute outflow Mach numbers at the center of the channel. It is clear from this figure that the rotor blade absolute outflow Mach number at the design corrected revolution speed and the design corrected ex-

(key to Fig. 9 on next page)

Key to Fig. 9.

1. Corrected flow rate
2. Ratio of experimental corrected revolution speed to design corrected revolution speed
3. Corrected expansion ratio

pansion ratio is 0.375. This value agrees well with the design value.

(f) Velocity Triangle (Fig. 14)

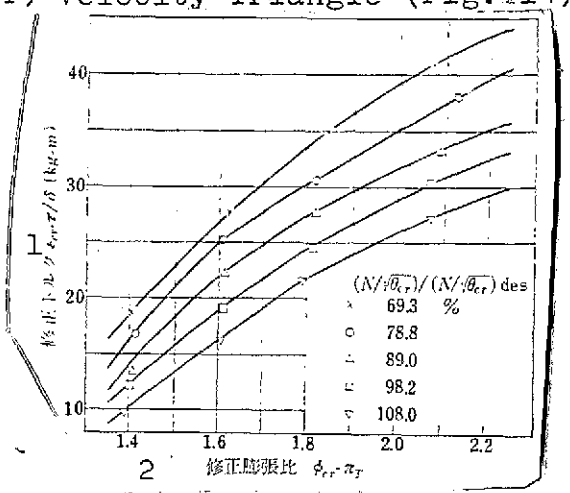

Fig. 10. Torque characteristics

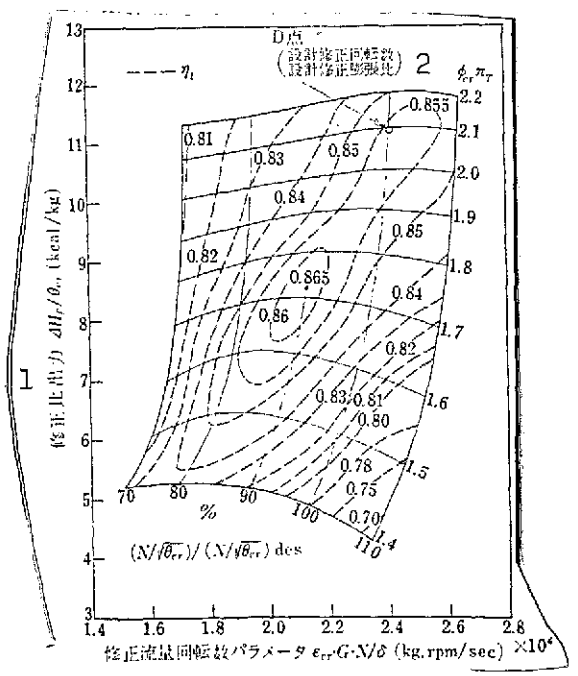

Fig. 11. Map of overall performance

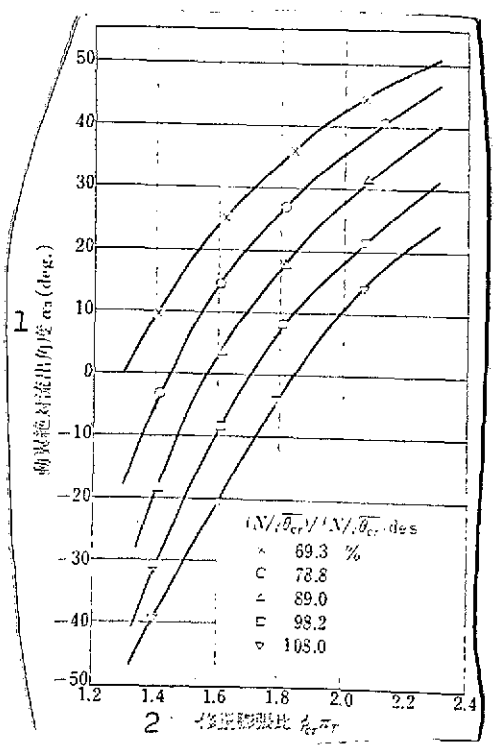

Fig. 12. Rotor blade absolute outflow angle (MEAN)

(Keys on following page)

Key to Fig. 10.

1. Corrected torque
2. Corrected expansion

Key to Fig. 11.

1. Corrected specific output
2. Point D
   (design corrected revolution speed)
   (design corrected expansion ratio)
3. Corrected flow rate revolution speed parameter

Key to Fig. 12

1. Rotor blade absolute outflow
2. Corrected expansion ratio

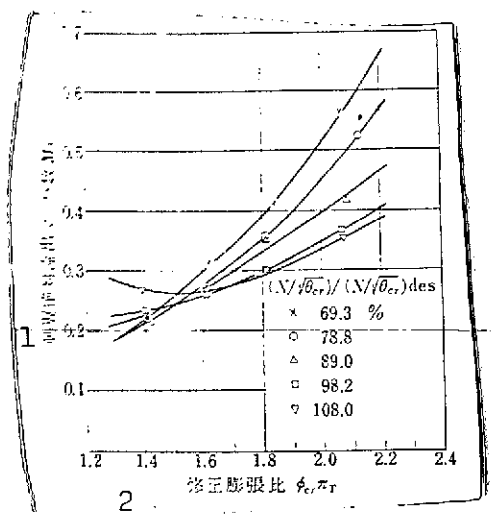

Fig. 13. Rotor blade absolute outflow Mach number (MEAN)

Key:

1. Rotor blade absolute outflow Mach number
2. Corrected expansion ratio

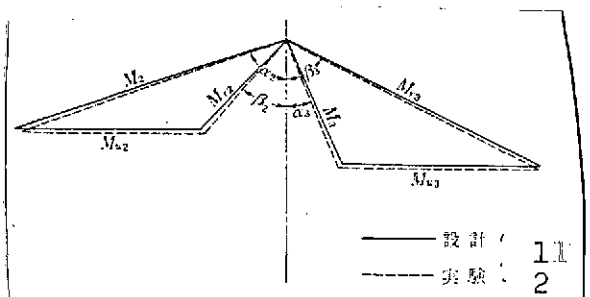

	記号	設計値	実験値
マッハ数	M_2	0.8013	0.785
	M_3	0.3750	0.375
	M_{r2}	0.3421	0.338
	M_{r3}	0.7726	0.766
	M_{a2}	0.2476	0.257
	M_{a3}	0.3448	0.349
	M_{u2}	0.5260	0.521
	M_{u3}	0.5439	0.545
	M_{2u}	0.7621	0.742
	M_{3u}	0.1475	0.137
	M_{r2u}	0.2361	0.221
	M_{r3u}	0.6914	0.682
角度 (deg)	α_2	72.0	70.9
	α_3	23.2	21.5
	β_2	43.6	40.7
	β_3	63.5	62.9

Fig. 14. Comparison of velocity triangle (comparison with design)

1. Design
2. Experiment
3. Symbol
4. Design value
5. Experimental value
6. Mach number
7. Angle (deg)

Using the experimental results obtained as described above, we sought the velocity triangle at the point of the design corrected revolution speed and the design corrected expansion ratio. That is, we calculated the velocity triangles at the stator blade outlet and the rotor blade outlet using the experimental values of the flow rate and specific output at this point, of the rotor blade absolute outflow angle at the MEAN position, and of the rotor blade absolute outflow Mach number, as well as the annulus area at the stator blade outlet and the total pressure loss coefficient of the stator blades. The only hypothesis in these calculations was that it was assumed that the total pressure loss coefficient of the stator blades (Y_{tN}) was 0.0874. This value consists of the profile loss obtained by means of blade cascade experiments to which the secondary flow loss calculated in accordance with item [10] in the bibliography was added. Let us add that, even though this hypothetical value may be somewhat different from the actual value, there are not very great differences in the velocity triangles which are obtained. /18

In Fig. 14, the experimental velocity triangles obtained in this way are shown in comparison with the design velocity triangles at the mean blade diameter. According to this figure, the outflow angle of the stator blade is about 1.1° smaller than the design outflow angle, and this indicates that the flow has risen to this extent in the axial direction. In this manner, in the stator blades, the flow cannot be curved as much as was anticipated (decrease of the deflection angle), while at the same time, there is also a decrease in the expansion ratio inside the stator blades (under-expanding), as is clear from the absolute outflow Mach number. On the other hand, it is clear that the deflection angle of the rotor blade has also decreased about 3.5° from the design value.

(g) Internal Flow (Fig. 15)

The internal flow at the rotor blade outlet was measured

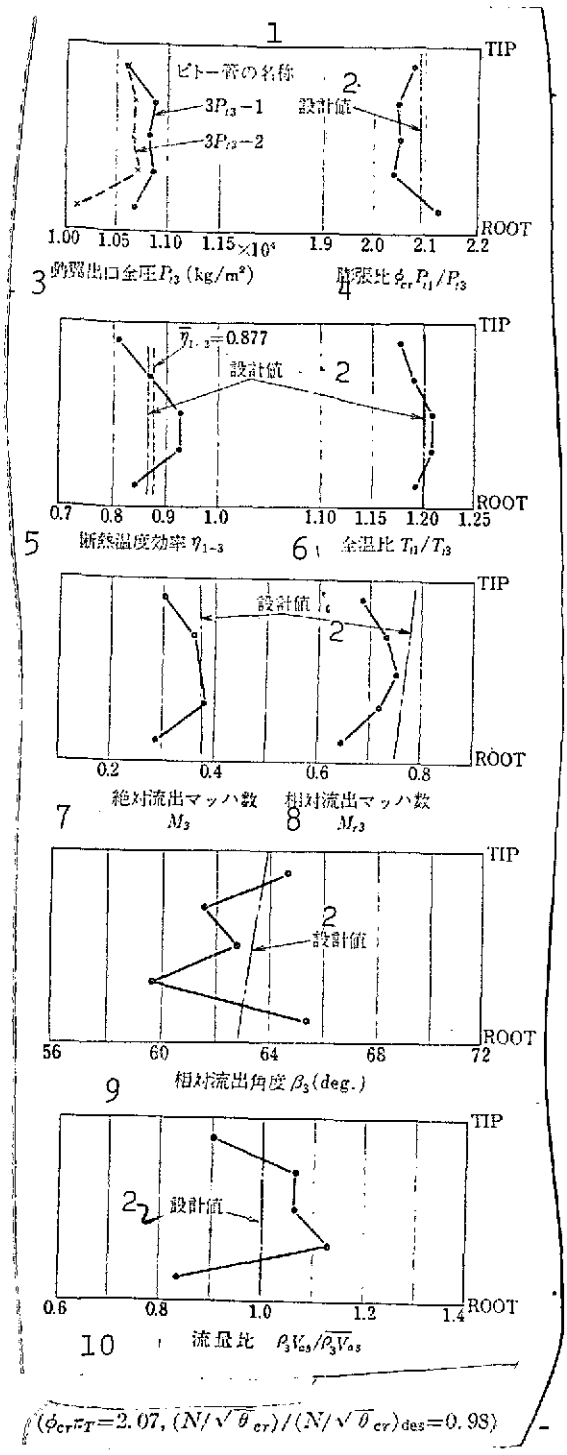

Fig. 15. Internal flow

Key:

1. Appellation of Pitot tube
2. Design value
3. Rotor blade outlet total pressure

(Key cont'd. on next page.)

at approximately the design corrected revolution speed and the design corrected expansion ratio. The results of the measurements are shown in Fig. 15.

The distribution of the rotor blade outlet total pressure P_{t3} plotted exactly the total pressure distribution as traversed by the two Pitot tubes installed in the circumferential direction. As is shown in this example, the measured values are not uniform in the circumferential direction, but there is a certain amount of distribution. In the following let us express the distribution in the radial direction in terms of these local mean values (the mathematical mean values of the measured values at the identical blade height). It is clear from a glance at Fig. 15 /17 that the measured values all differ considerably in the radial direction.

As is seen in the distribution of the expansion ratio and the total temperature ratio, there is a greater drop in the total pressure near the walls than there is in the vicinity of the center of the channel.

Key to Fig. 15, continued:

4. Expansion ratio
5. Adiabatic temperature efficiency
6. Total temperature ratio.
7. Absolute outflow Mach number
8. Relative outflow Mach number
9. Relative outflow angle
10. Flow rate ratio

However, there is a small thermal head, as is seen in the distribution of the total temperature ratio. Consequently, the adiabatic temperature efficiency also is quite low near the walls. The mass flow rate mean value of this efficiency (as is shown in the flow rate ratio distribution, the flow rate differs considerably in the radial direction; therefore, the value was averaged by applying the weight of the flow local efficiency in the radial direction) is 0.877. This value in itself satisfies the design specifications, but one should note carefully that there are local values which differ considerably from the design value.

On the other hand, in the distribution of the blade outflow Mach numbers, it is indicated that the flow velocity is slow near the walls. Furthermore, the distribution of the relative outflow angles also has some complex shapes which are seen nowhere else.

The distribution in the radial direction of the flow rate per unit area was also calculated using the above local values of the measured values. It was shown in terms of the flow rate ratio with respect to the mean flow rate per unit area. It is clear from this that there are big differences in the flow rate in the radial direction and that it is quite small in the vicinity of both walls. If this fact as well as the total temperature ratio distribution above are taken into consideration, it is clear that the amount of work also is quite small at the blade tip part and the blade root part as compared with the vicinity of the mean blade diameter.

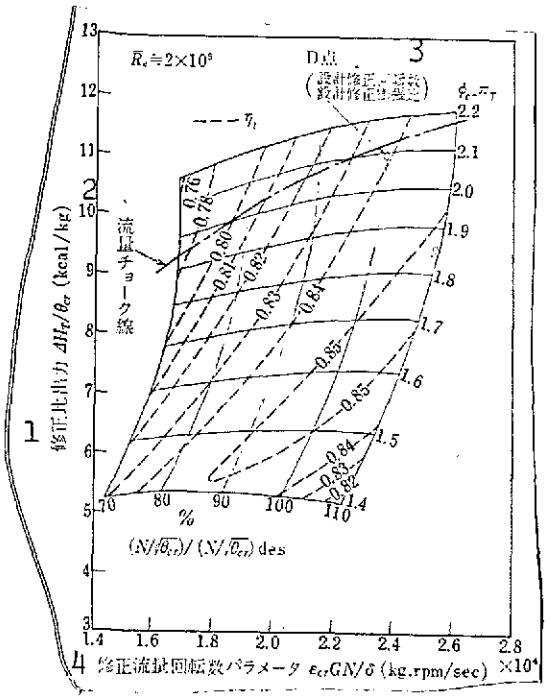

Fig. 16. Map of overall performance by calculations [10]

Key:

1. Corrected specific output
2. Flow rate choke line
3. Point D (design corrected revolution speed)
4. (design corrected expansion ratio)
4. Corrected flow rate revolution speed parameter

3.5. Studies and Discussion of the Experimental Results

In these experiments, a quite good turbine adiabatic efficiency was obtained throughout almost all regions of the experiments. In these experiments, the mean Reynolds number in the turbine at the design corrected revolution speed and the corrected expansion ratio (using the Reynolds number as defined in item [10] in the bibliography) was approximately 4.3×10^5. On the other hand, the number at the design conditions was approximately 1.1×10^5. Therefore, it is assumed that, because of these differences in the Reynolds numbers, at the design operating conditions there will be a decrease of about 2-3% from the adiabatic efficiency of these experiments.[1] These design operating conditions were adjusted to the operating conditions

[1] Concerning the effects of the Reynolds number on the turbine efficiency, various formulas, most of them empirical formulas, have been proposed. Although there are some differences between these formulas, when the Reynolds' number is less than 2×10^5 its influence on the efficiency may generally be expressed in terms of the law of approximately -0.2 power of the Reynolds number. As the Reynolds number becomes greater, its influence becomes less, and when the value is approximately $10^6 - 10^7$, it is believed that its influence is entirely negligible.

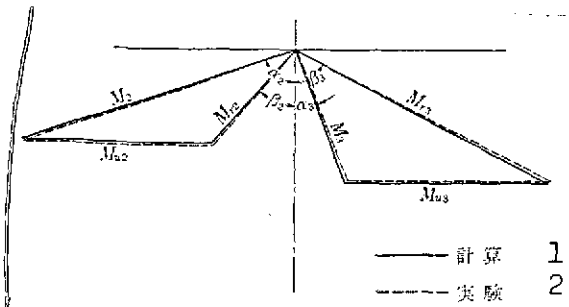

記号 3		計算値 4	実験値 5
6 マッハ数	M_2	0.778	0.785
	M_3	0.377	0.375
	M_{r2}	0.333	0.338
	M_{r3}	0.760	0.766
	M_{a2}	0.251	0.257
	M_{a3}	0.353	0.349
	M_{u2}	0.517	0.521
	M_{u3}	0.540	0.545
	M_{2u}	0.737	0.742
	M_{3u}	0.133	0.137
	M_{r2u}	0.220	0.221
	M_{r3u}	0.673	0.682
7 角度 (deg)	α_2	71.2	70.9
	α_3	20.6	21.5
	β_2	41.2	40.7
	β_3	62.3	62.9

Fig. 17. Comparison of velocity triangle (comparison with calculations)[10]

Key:

1. Calculation
2. Experiment
3. Symbol
4. Calculated values
5. Experimental values
6. Mach number
7. Angle

of high-temperature tests using actual model turbines [11] which were performed separately at our Prime Mover Department. In this case, since the pressure and temperature at the turbine inlets are considerably less uniform than in these experiments, it is believed that there is some further decrease in the efficiency [10]. In view of these facts, when operated at the design conditions, it is assumed that the adiabatic efficiency of this turbine will be approximately 82-83%. /18 However, when this high-temperature turbine is actually adopted in an airplane, the turbine inlet total pressure will not be as low as that in these design conditions, but will have a value several times greater or even more. Therefore, the mean Reynolds number inside the turbine will also increase together with it, and it is believed that it will be approximately the same as, or even larger than, the Reynolds number in these experiments. Thus, even when one keeps in mind the lack of uniformity of the gaseous states at the turbine inlet, it is believed that, in the actual engines, the required

efficiency of 85% will be satisfied.

On the other hand, the turbine inlet flow rate departs considerably from the design specifications. As is pointed out also in [10] in the bibliography, this flow rate is extremely sensitive to the blade mounting angle, that is to the blade throat area. Especially in the upstream blades, deviations in this angle have a big effect on the flow rate. It is assumed from this that, since the blade mounting angle was pronounced in the axial direction during the manufacture of this turbine, the throat area increased as a result, and there was a considerable flow rate as in the experiments. In actual fact, it has been ascertained that in this turbine the measured values of the throat area of the stator blades are 5.0% greater than the values which were planned during designing. Incidentally, when these measured areas are used to calculate the performance of the turbine, the results are as shown in Fig. 16. At point D, that is, the point of the design corrected revolution speed and the design corrected expansion ratio, the flow rate is about 5.4% greater than the design flow rate, and this excess flow rate is close to the amount obtained in the experiments. Besides, a deviation in the blade mounting angle is also assumed from the stator blade outflow angle in the diagram of the velocity triangle (Fig. 14) obtained in the experiments. Furthermore, the velocity triangle at point D in Fig. 16, which was calculated using the measured throat area, agrees well with that of the experiments, as is shown in Fig. 17. It may be concluded from the preceding that the main cause of the excessive flow rate in the experiments is the following. That is, since the setting angle for mounting the stator blades deviated about 1°, the throat area became excessively large as a result. In this manner, in stator blades of an air-cooled turbine, in which it is necessary to select a large outflow angle, a slight deviation in the mounting angle will have a great

influence on the flow rate. Therefore, it is especially necessary to pay careful attention to this point.

In the experimental results for the internal flow, the various experimental values had a considerable distribution in the radial direction, and locally they displayed values which differed from the design values. In particular, it is thought that the complicated shapes of the relative outflow angles of the rotor blade were probably caused by the secondary flow or the flow from the blade tip clearance. When these /19 results for the internal flow are considered in connection with the results for the overall performance as described above, the following may be said concerning the design. That is, the hypotheses (or the designing methods) used in designing this turbine locally do not agree with the actual flow, but when viewed in terms of the overall performance they may be called valid hypotheses (or designing methods) in the average sense. Nevertheless, in future designing it will be necessary to make improvements while taking this actual flow into consideration.

4. Conclusion

An air-cooled turbine was designed and manufactured with a turbine inlet total temperature of 1,150°C as the target, and experiments were performed here without supplying blade cooling air in order to examine its aerodynamic performance. Studies were made of the overall performance and of the internal flow. The ranges of the experiments were a revolution speed of approximately 70-110% and a turbine expansion ratio of 1.4-2.1.

The conclusions concerning the design obtained from these experimental results were the following:

(1) It was learned that even air-cooled turbines which are subject to various restrictions in their blade shape or other items because of the necessity of passing cooling

air inside the blades can be designed and manufactured, without any impairment of their performance, by applying the design techniques used in the past in non-cooled turbines, under a number of basic policies which are required in air-cooled blades.

The chief experimental results were the following:

(2) Within the range of the experiments, this air-cooled turbine displayed an adiabatic efficiency of 0.7-0.865. The maximum adiabatic efficiency of 0.865 was obtained at a revolution speed in the vicinity of 90% and at an expansion ratio in the vicinity of 1.72

(3) In this air-cooled turbine, the specific output obtained at the design revolution speed and the design expansion ratio was approximately the same as that in the design. The adiabatic efficiency at that time was 0.865, and the adiabatic temperature efficiency (mass flow rate mean value) was 0.877.

(4) The flow rate of this air-cooled turbine was choked by the rotor blade, and the expansion ratio at which it was thought that choking was performed for all revolution speeds in the experiments was approximately 2.3.

(5) The turbine flow rate at the design revolution speed and the design expansion ratio was approximately 7.3% greater than the design value. It is believed that this is chiefly because the throat area of the stator blades was greater than the design value. In blades with a rather great outflow angle such as these stator blades, careful attention must be paid when setting the throat part.

(6) The torque limit of the turbine does not yet occur within the range of operations in the experiments.

(7) As for the work distribution in the blade height direction at the design revolution speed and the design expansion ratio, it is small near the TIP and the ROOT and great near the MEAN. However, it was learned that the designed work is given out by the blade as a whole.

The following problems are left for the future:

(8) The hypothesis for the flow inside the turbine used in this design coincides on the average with the actual flow, but it cannot be said to coincide locally. In the future, it will be necessary to make improvements in the design, taking into consideration these real flow phenomena.

(9) Since it is thought that the cooling air has an influence on the turbine flow, and consequently on the aerodynamic performance, it will be necessary to perform designing and experimentation in which this influence is also taken into consideration.

(10) In the actual machinery, it is anticipated that there will be considerable thermal deformations, not only in the blades, but also in the various turbine parts, and it is believed that, in short blades such as these air-cooled blades, they would have a relatively great influence on the performance properties of the rotor blade tip clearance. More detailed experiments are necessary for individual blades in order to clarify the various performance properties of the air-cooled turbine and air-cooled blades, including these questions.

Post Postscript

The co-operation of the following persons was obtained in this research. The writers take this opportunity to express their gratitude to them.

Director Matsumoto, Prime Mover Department; laboratory director Shimazaki; laboratory director Nishio; technical official Koshinuma (mensuration); technical officials Kokura, Shimodaira, and Yamada (air sources); and the Technical Development Laboratory, Aircraft Engines Department, Ishikawajima-Harima Heavy Industries Co., Ltd. (designing, manufacturing).

REFERENCES

1. Yamamoto, Atsumasa, and Takahara, Kitao: "A consideration of the flow rate of turbine cooling air and of the performance properties of turbofan engines," Dai-11-kai koku gendoki ni kan-suru koenkai koen shu [Lectures delivered at the 11th lecture meeting concerning aircraft prime movers], 1971.

2. Warren J. Whitney, Edward M. Szanca, Thomas P. Moffitt and Daniel E. Monreo: Cold-Air Investigation of a Turbine for High-Temperature-Engine Application. I. Turbine Design and Overall Stator Performance, NASA TN D-3751, 1966.

3. Herman W. Prust, Jr., Harold J. Schum, and Frank P. Behning: Cold-Air Investigation of a Turbine for High-Temperature-Engine Applicaiton. II. Detailed Analytical and Experimental Investigation of Stator Performance, NASA TN D-4418, 1967. /20

4. Warren J. Whitney, Edward M. Szanca, Bernard Bider, and Daniel E. Monreo: Cold-Air Investigation of a Turbine for High-Temperature-Engine Application III. Overall Stage Performance, NASA TN D-4389, 1967.

5. Hatta, Keizo, Matsunoki, Masakatsu and Torisaki, Tadao, ed.: Kitai kikai handobukku [Gas machinery handbook], Asakura Shoten, 1968, p. 603.

6. George E. Glawe, Frederick S. Simmons, and Truman M. Stickney: Recovery Corrections and Time Constants of Several Chromel-Alumel Thermocouple Problems in High-Temperature, High-Velocity Gas Streams, NASA TN 3766, 1956.

7. Fujii, Shoichi, Nishiwaki, Hideo, Yoshida, Akira, Gomi, Mitsuo, Takeda, Katsumi and Sugawara, Noboru: "Studies of high-speed single-stage axial flow compressors," Koku Uchu Gijutsu Kenkyusho hokoku [Technical report of National Aerospace Laboratory], TR-134, 1967.

8. Matsunoki, Masakatsu, Torisaki, Tadao, Nishio, Kenji, Takahara, Kitao et al.: Jido keisoku no tame no chikara heiko-gata atsuryoku henkanki no shisaku kenkyu [Prototype studies of a force-balancing type pressure converter for automatic measurements], National Aerospace Laboratory.

9. Torisaki, Tadao, Nose, Hiroyuki, Morita, Mitsuo, Inoue, Shigeo, and Sekine, Shizuo: "Studies of transonic axial flow turbines (I)," Koku Uchu Gijutsu Kenkyusho hokoku [Technical report of National Aerospace Laboratory], TR-272, 1972.

10. D.G. Ainley and G.C.R. Mathieson; A Method of Performance Estimation for Axial Flow Turbines, ARC R & M. No. 2974, 1951.

11. Takahara, Kitao, Nose, Hiroyuki, Torisaki, Tadao, Nashio, Kenji and Suzuki, Kunio: Koon tabin shiken setsubi [High temperature turbine testing equipment], preprint for the 1969 National Aerospace Laboratory research meeting, 1969.

12. Oba, Jiro: Joki oyobi gasu tabin [Steam and gas turbines], Nikkan Kogyo Shimbun Sha, 1958, pp. 85-87.

13. M.S. Chappel and E.P. Cockshutt; Gas Turbine Cycle Calculations: Thermodynamic Data Tables for Air and Combustion Products. National Research Council of Canada. Aeronautical Report R-51, 1969.

14. D. Fielding and J.E.C. Topps; Thermodynamic Data for the Calculation of Gas Turbine Performance, ARC R & M. No. 3099, 1959.

15. D.G. Ainley and G.C.R. Mathieson; Examination of the Flow and Pressure Losses in Blade Row of Axial-Flow Trubines, ARC R&M. No. 2891, 1951.

16. For example, Kodo, Yoshio: Dennetsu gairon [Introduction to heat transfer], third ed., Yokendo, 1967, pp. 394-416.

17. James W. Miser, Warner L. Stewart, and Daniel E. Monreo: Effect of High Rotor Pressure-Surface Diffusion on Performance of a Transonic Turbine, NACA RM E 55 H 29 a, 1955.

18. Ascher, H. Shapiro; The Dynamics and Thermodynamics of Compressible Fluid. Vol. 1, The Ronald Press Company, New York.

19. James C. Dunavant and John R. Erwin; Investigation of a Related Series of Turbine-Blade Profiles in Cascade, NACA TN 3802.

20. Stechkin: Jetto enjin riron, tabo kikai [Jet engine theory, turbo machinery], tr. by Hamashima, Misao. Korona Sha, 1969, pp. 271-283.

21. William E. Berkey: Overall Performance of the J 71 Three-Stage Turbine, NACA RM E 52B29, 1952.

22. D.G. Ainley: Estimation of the Change in Performance Characteristics of a Turbine Resulting from Changes in the Gas Thermodynamic Properties, ARC R & M. No. 2973, 1951.

23. J. Dunham and P.M. Came: Improvements to the Ainley-Mathieson Method of Turbine Performance Prediction, ASME Paper No. 70-GT-2, 1970.

29. Takahara, Kitao, Yamamoto, Atsumasa, Inoue, Shiegeo, Usui, Hiroshi and Mimura, Fujio: "Aerodynamic performance of air-cooled turbines (Part I)," Dai-12-kai koku gendoki ni kan-sura koenkai koen shu [Lectures delivered at the 12th lecture meeting concerning aircraft prime movers], 1972.

APPENDIX A. DETAILS OF THE DESIGN

Details of the aerodynamic design of these turbines are shown below. The hypotheses in the calculations used here as well as the fundamental policies for determining the blade profiles and blade arrangements are those described in the main text.

1. Calculating Turbine Performance Properties (Single-Dimensional Calculations)

The fundamental equations used in the calculations are the following:

(1) equation for the relationship between the total temperature and the static temperature at the same point:

$$\frac{T_t}{T_s}=1-\frac{\kappa-1}{2}M^2 \tag{1.1}$$

(2) equation for the relationship between the total pressure and the static pressure at the same point:

$$\frac{P_t}{P_s}=\left(1+\frac{\kappa-1}{2}M^2\right)^{\frac{\kappa}{\kappa-1}} \tag{1.2}$$

(3) equation for sound velocity a:

$$a=\sqrt{\kappa\cdot g\cdot R\cdot T_s} \tag{1.3}$$

(4) equation defining velocity coefficient of stator blade ϕ_N:

$$\varphi_N=\frac{V_2}{V_{2ad}} \tag{1.4}$$

Here, V_2 is the actual outflow velocity of the stator blade, and V_{2ad} is the theoretical outflow velocity due to the adiabatic thermal head.

(5) equation defining total pressure loss coefficient of rotor blade Y_{tR}:

$$Y_{tR}=\frac{P_{r2}-P_{r3}}{P_{r3}-P_{s3}} \tag{1.5}$$

Here, the subscript r (used for the temperature and pressure) indicates a state of relative damming towards the blades. That is, P_{r2}, P_{r3} and P_{s3} are the relative total pressure at the rotor blade inlet, the relative total pressure at the rotor blade outlet, and the static pressure at the rotor blade outlet, respectively.

(6) equation for flow rate: If a single-dimensional current is assumed, the turbine flow rate will be obtained by the following equation:

$$G=\gamma \cdot V \cdot A \tag{1.6}$$

Here, A is the channel sectional area orthogonal to flow velocity V.

The chief equations which are derived from the above fundamental equations and which are used in the calculations are the following. When equation (1.6) is written in the form of a dimensionless flow rate using equations (1.1)-(1.3), the following equation will be obtained:

$$\frac{G\sqrt{T_t}}{A \cdot P_t}=\sqrt{\frac{\kappa \cdot g}{R}}M\Big/\left(1+\frac{\kappa-1}{2}M^2\right)^{\frac{\kappa+1}{2(\kappa-1)}} \tag{1.7}$$

When the relative outflow Mach number of the rotor blade M_{r3} is calculated, the necessity of seeking it numerically arises. That is, using the continuous conditions $G_2 = G_3$ and the adiabatic hypothesis $T_{r2} = T_{r3}$, we obtain the following from equation (1.7):

$$\frac{\left(1+\frac{\kappa-1}{2}M_{r3}^2\right)^{\frac{\kappa+1}{2(\kappa-1)}}}{M_{r3}}\cdot\frac{P_{r2}}{P_{r3}}=\frac{A_3}{A_2}\times\frac{\left(1+\frac{\kappa-1}{2}M_{r2}^2\right)^{\frac{\kappa+1}{2(\kappa-1)}}}{M_{r2}} \tag{1.8}$$

Here, A_2 and A_3 are the actual channel areas at right angles to the flow at the rotor blade inlet and outlet, respectively. In this case, since the annular areas are identical in both places, the area ratio A_3/A_2 is expressed by the following equation:

$$\frac{A_3}{A_2}=\frac{\cos\beta_3}{\cos\beta_2} \tag{1.9}$$

On the other hand, the ratio P_{r2}/P_{r3} of the relative total pressure before and after the rotor blade is expressed by the following equation, using equations (1.2) and (1.5):

$$\frac{P_{r2}}{P_{r3}}=1+Y_{tR}\left\{1-\left(1+\frac{\kappa-1}{2}M_{r3}^2\right)^{-\frac{\kappa}{\kappa-1}}\right\} \tag{1.10}$$

Consequently, the following equation will be obtained if we eliminate A_3/A_2 and P_{r2}/P_{r3} from equations (1.8)-(1.10).

$$\frac{\left(1+\frac{\kappa-1}{2}M_{r3}^2\right)^{\frac{\kappa+1}{2(\kappa-1)}}}{M_{r3}}\times\left[1+Y_{tR}\left\{1-\left(1+\frac{\kappa-1}{2}M_{r3}^2\right)^{-\frac{\kappa}{\kappa-1}}\right\}\right]=\frac{\cos\beta_3}{\cos\beta_2}\cdot\frac{\left(1+\frac{\kappa-1}{2}M_{r2}^2\right)^{\frac{\kappa+1}{2(\kappa-1)}}}{M_{r2}} \tag{1.11}$$

M_{r3} is sought from this equation by finding a numerical solution.

Furthermore, the total temperature ratio before and after the turbine is expressed by the following equation on the basis of equation (1.1), taking into consideration the adiabatic hypothesis.

$$\frac{T_{t3}}{T_{t1}}=\frac{\left(1+\frac{\kappa-1}{2}M_3^2\right)\left(1+\frac{\kappa-1}{2}M_{r2}^2\right)}{\left(1+\frac{\kappa-1}{2}M_{r3}^2\right)\left(1+\frac{\kappa-1}{2}M_2^2\right)} \tag{1.12}$$

The (total pressure/static pressure) ratio P_{t1}/P_{s2} before and after the stator blades, on the basis of equations (1.1)-(1.4), will be the following, taking into consideration the fact that ϕ_N is close to 1:

$$\frac{P_{t1}}{P_{s2}}=\left\{1+\frac{\frac{\kappa-1}{2}\left(\frac{M}{\varphi_N}\right)^2}{1+\frac{\kappa-1}{2}M^2\left(1-\frac{1}{\varphi_N^2}\right)}\right\}^{\frac{\kappa}{\kappa-1}} \fallingdotseq\left\{1+\frac{\kappa-1}{2}\left(\frac{M}{\varphi_N}\right)^2\right\}^{\frac{\kappa}{\kappa-1}} \tag{1.13}$$

The total pressure ratio before and after the turbine may be expressed by the following equation, utilizing this equation as well as equations (1.2) and (1.10);

$$\frac{P_{t3}}{P_{t1}}=\left\{\frac{\left(1+\frac{\kappa-1}{2}M_3^2\right)\left(1+\frac{\kappa-1}{2}M_{r2}^2\right)}{\left(1+\frac{\kappa-1}{2}M_{r3}^2\right)\left(1+\frac{\kappa-1}{2}\frac{M_2^2}{\varphi_N^2}\right)}\right\}^{\frac{\kappa}{\kappa-1}} \times\left[1+Y_{tR}\left\{1-\left(1+\frac{\kappa-1}{2}M_{r3}^2\right)^{-\frac{\kappa}{\kappa-1}}\right\}\right]^{-1} \tag{1.14}$$

Using the total temperature ratio and the total pressure ratio before and after the turbine, the adiabatic temperature efficiency of the turbine η_{1-3} is defined by the following equation: /22

$$\eta_{1-3}=\frac{1-(T_{t3}/T_{t1})}{1-(P_{t3}/P_{t1})^{\frac{\kappa-1}{\kappa}}} \tag{1.15}$$

The thermal head inside the turbine ΔH_T is defined and sought by the following equation:

$$\Delta H_T = \frac{(W_{2u} + W_{3u})U}{g \cdot J} = \frac{(V_{2u} + V_{3u})U}{g \cdot J} \tag{1.16}$$

Furthermore, the turbine flow rate is calculated by the following equation. That is, if we take into consideration that $T_{t1} = T_{t2}$ and $A_2 = A_{a2}\cos\alpha_2$, the flow rate G will be as follows on the basis of equation (1.7):

$$G = \frac{\frac{P_{t2}}{\sqrt{T_{t2}}} A_{a2} \cos\alpha_2 \sqrt{\frac{\kappa \cdot g}{R}} M_2}{\left(1 + \frac{\kappa - 1}{2} M_2^2\right)^{-\frac{\kappa+1}{2(\kappa-1)}}} \tag{1.17}$$

Here, P_{t2} is sought from the following equation. On the basis of equations (1.1)-(1.4), the total pressure ratio before and after the stator blades will be: /23

$$\frac{P_{t2}}{P_{t1}} = \left[1 + \frac{\kappa - 1}{2} M_2^2 \left\{1 - \left(\frac{1}{\varphi_N}\right)^2\right\}\right]^{\frac{\kappa}{\kappa-1}} \tag{1.18}$$

The sequence and results of these calculations are shown in Appendix Table 1.

2. Calculation of Velocity Triangles (Two-Dimensional Calculations)

The fundamental equations for a single streamline are as follows. From hypothesis (1), it is assumed that the interior of the turbine is adiabatically insulated from the outside. Therefore,

$$H_{t1} = H_{t2} = H_{t3} + \Delta H_T \tag{2.1}$$

Furthermore, since the gas is treated as a perfect gas,

APPENDIX TABLE 1. SEQUENCE AND RESULTS OF CALCULATIONS OF TURBINE PERFORMANCE

CALCULATING CONDITIONS:

T_{t1}=1423.2 °K　　B_{LR}=46.0 deg.
N=13300 r. p. m　　φ_N=0.97
M_2=0.80　　Y_{tR}=0.23
α_2=72.0 deg.　　r_M=0.2633 m
β_3=63.5 deg.　　κ=1.315

No	Object to be calculated	Calculating equations, etc.	Calculated value	Unit
1	U	$2\pi r_M \cdot N/60$	3.667179+02	m/sec
2	T_{t2}	T_{t1}	1.423200+03	°K
3	T_{s2}	②, M_2→Eq(1·1)	1.292878+03	°K
4	a_2	③→Eq(1·3)	6.983386+02	m/sec
5	V_2	$M_2 \times$ ④	5.586709+02	m/sec
6	M_{u2}	①/④	5.251291−01	
7	M_{r2u}	$M_2 \cdot \sin\alpha_2$ − ⑥	2.357159−01	
8	M_{a2}	$M_2 \cdot \cos\alpha_2$	2.472142−01	
9	M_{r2}	$\sqrt{⑦^2+⑧^2}$	3.415799−01	
10	β_2	$\tan^{-1}(⑦/⑧)$	4.363619+01	deg.
11	A_3/A_2	$\cos\beta_3/\cos⑩$	6.165203−01	
12	M_{r3}	⑨, ⑪, Y_{tR}→Eq(1·11)	7.732300−01	
13	T_{r3}	⑥, ⑨→Eq(1·1)	1.316637+03	°K
14	T_{s3}	⑫, ⑬→Eq(1·1)	1.203323+03	°K
15	a_3	⑭→Eq(1·3)	6.737185+02	m/sec
16	W_3	⑫×⑮	5.209393+02	m/sec
17	W_{3u}	⑯·sin β_3	4.662063+02	m/sec
18	W_2	④×⑨	2.385384+02	m/sec
19	W_{2u}	⑱·sin⑩	1.646095+02	m/sec
20	ΔW_u	⑰+⑲	6.308158+02	m/sec
21	ΔH_T	①×⑳/$g \cdot J$→Eq(1·16)	5.529457+01	kcal/kg
22	M_{u3}	①/⑮	5.443192−01	
23	M_{3u}	⑫·sin β_3 − ㉒	1.476705−01	
24	M_{a3}	⑫·cos β_3	3.450143−01	
25	M_3	$\sqrt{㉓^2+㉑^2}$	3.752885−01	
26	T_{t3}/T_{t1}	⑨, ⑫, ㉕, M_2→Eq(1·12)	8.642610−01	
27	P_{t3}/P_{t1}	⑨, ⑫, ㉕, M_2, φ_N, Y_{tR}→Eq(1·14)	4.951532−01	
28	η_{1-3}	㉕, ㉖→Eq(1·15)	8.759679−01	
29	i_R	⑩ − B_{LR}	−2.363808+00	deg.
30	V_{a3}	⑮×㉔	2.324425+02	m/sec

$$P_s = \gamma \cdot R \cdot T_s \qquad (2.2)$$

$$a = \sqrt{\kappa \cdot g \cdot R \cdot T_s} \qquad (2.3)$$

$$M = V/a \tag{2.4}$$

$$H_t = H_s + \frac{V^2}{2g \cdot J} \tag{2.5}$$

$$dH = c_p \cdot dT \tag{2.6}$$

$$dS = c_p \frac{dT_s}{T_s} - \frac{R}{J} \frac{dP_s}{P_s} \tag{2.7}$$

$$c_p = \frac{\kappa}{\kappa - 1} \frac{R}{J} \tag{2.8}$$

The fundamental equations for intervals between streamlines use the following conditional equation for the radial balance [12]:

$$\frac{1}{\rho} \cdot \frac{dP_s}{dr} = \frac{V_u^2}{r} - \frac{dV_{rad}}{dt} \tag{2.9}$$

The chief equations which are derived from the above fundamental equations and from hypothesis 2.2 in the main text and which are used in calculations are the following.

On the basis of hypothesis (2), the radial position (r_1, r_2, r_3) of the streamlines between the turbine stages can be written as follows:

$$r_1 = r_2 = r_3 = r. \tag{2.10}$$

If the radial direction velocity component is regarded as minute and is disregarded, equation (2.9) will assume the following form (simple radial balance):

$$\frac{g}{\gamma} \cdot \frac{dP_s}{dr} = \frac{V_u^2}{r} \tag{2.11}$$

On the basis of hypothesis (3), we may use equations (2.1) and (2.5):

$$\frac{dH_{t1}}{dr_1} = \frac{dH_{t2}}{dr_2} = \frac{dH_{s2}}{dr_2} + \frac{1}{2g \cdot J} \cdot \frac{dV_2^2}{dr_2} = 0 \tag{2.12}$$

On the basis of hypothesis (4), we may use equations (2.2), (2.6) and (2.7):

$$T_{s2}\frac{dS_2}{dr_2}=\frac{dH_{s2}}{dr_2}-\frac{1}{J\cdot\gamma_2}\cdot\frac{dP_{s2}}{dr_2}=0 \tag{2.13}$$

On the basis of hypothesis (5),

$$\frac{d\alpha_2}{dr_2}=0 \tag{2.14}$$

On the basis of hypothesis (6), we may use equation (2.11):

$$\frac{g}{\gamma_2}\cdot\frac{dP_{s2}}{dr_2}=\frac{V_{2u}^2}{r_2} \tag{2.15}$$

Therefore, from equations (2.12), (2.13), and (2.15), we obtain:

$$-V_2\frac{dV_2}{dr_2}=\frac{V_{2u}^2}{r_2} \tag{2.16}$$

If the above equation is transformed using equation (2.14) and $V_{2u} = V_2\sin\alpha_2$, we will obtain the equation for the radial direction distribution of the flow velocity at the stator blade outlet. That is,

$$\begin{aligned} &V_2r_2^m=\text{const.}\\ &V_{2u}r_2^m=k_1\text{(const.)}\\ &V_{2a}r_2^m=\text{const.} \end{aligned} \tag{2.17}$$

Here,

$$m=\sin^2\alpha_2$$

Furthermore, if hypothesis (7) and equation (2.10) are taken into consideration, the following equation will apply.

$$(V_{2u}+V_{3u})r=\frac{g\cdot J\cdot\Delta H_T}{\omega}=k_2\text{(const.)} \tag{2.18}$$

Here ω is the angular velocity and $\omega = 2\pi N/60$ (N: rpm).

Therefore, if we take into consideration

$$\frac{d(\Delta H_T)}{dr} = 0 \tag{2.19}$$

we obtain the following equation from equations (2.1), (2.5), (2.10) and (2.12):

$$\frac{dH_{ts}}{dr_3} = \frac{dH_{ss}}{dr_3} + \frac{1}{2g \cdot J} \cdot \frac{dV_3^2}{dr_3} = 0 \tag{2.20}$$

On the basis of hypothesis (8), we may use equations (2.1), (2.6), (2.7) and (2.12):

$$T_{ss} \frac{dS_3}{dr_3} = \frac{dH_{ss}}{dr_3} - \frac{1}{J \cdot \gamma_3} \cdot \frac{dP_{ss}}{dr_3} = 0 \tag{2.21}$$

On the basis of hypothesis (9), we may use equation (2.11):

$$\frac{g}{\gamma_3} \cdot \frac{dP_{s3}}{dr_3} = \frac{V_{3u}^2}{r_3} \tag{2.22}$$

Therefore, on the basis of equations (2.20), (2.21) and (2.22), a similar equation to equation (2.16) can be obtained for the rotor blade outlet as well:

$$-V_3 \frac{dV_3}{dr_3} = \frac{V_{3u}^2}{r_3} \tag{2.23}$$

If we use $V_3^2 = V_{3a}^2 + V_{3u}^2$, the above equation will be

$$\frac{dV_{3a}^2}{dr_3} = -\frac{1}{r_3^2} \cdot \frac{d(r_3 V_{3u})^2}{dr_3} \tag{2.24}$$

Consequently, if we use equations (2.10), (2.17), and (2.18) and transform equation (2.24), we obtain:

$$\frac{d(V_{3a})^2}{dr}=2k_1^2(m-1)r^{-(2m+1)} -2k_1k_2(m-1)r^{-(m+2)} \tag{2.25}$$

If we integrate this and insert the initial conditions that $V_{2a} = V_{2aM}$ at $r = r_M$ (the subscript M indicates the value at MEAN), we can obtain the equation for the radial direction distribution of the axial flow velocity at the rotor blade outlet. That is, if we taken into consideration that $k_1 = V_{2uM}r_M^m$ and that $k_2 = (V_{2uM} + V_{3uM})\gamma M$, we obtain

/25

$$V_{3a}^2-V_{3aM}=\frac{1-m}{m}\cdot V_{2uM}^2\left\{\frac{1}{(r/r_M)^{2m}}-1\right\} -\frac{2(1-m)}{1-m}V_{2uM}(V_{2uM}-V_{3uM}) \times\left\{\frac{1}{(r/r_M)^{m+1}}-1\right\} \tag{2.26}$$

Furthermore, the fact that the gas inside the turbine is combustion gas was also taken into consideration, and the specific heat at constant pressure c_p was regarded as a function of the temperature and of the air-fuel ratio. That is, the specific heat at constant pressure of the air $c_{p,air}$ is first given as a function of the temperature.

$$c_{p\,air}=C_0+C_1T-C_2T^2+\cdots\cdots \tag{2.27}$$

Here, C_0, C_1, and C_2 are constants.

Since the enthalpy H at temperature T is:

$$H=\int_0^T c_p dT \tag{2.28}$$

the enthalpy of the air H_{air} at temperature T will be expressed by the following equation:

$$H_{air}=C_0T-\frac{C_1}{2}T^2+\frac{C_2}{3}T^3+\cdots\cdots-CH \tag{2.29}$$

Here, CH is a constant.

The pressure or temperature before and after the adiabatic change is sought using the following relative equation:

$$\log_{10}(P_2/P_1)=\phi_2-\phi_1 \tag{2.30}$$

Here, ϕ is the entropy function. It is expressed by the following equation:

$$\phi=(\log_{10}e)\frac{1}{R}\int_0^T\frac{c_p\cdot dT}{T} \tag{2.31}$$

Consequently, the entropy function of the air ϕ_{air} at the temperature T is expressed by the following equation using equation (2.27): /26

$$-\frac{C_2}{2}T^2+\cdots\cdots+CF\cdot R\Big) \tag{2.32}$$

Here, CF is a constant.

Thus, for the air one first seeks $c_{p\,air}$, H_{air} and ϕ_{air}. Then correction of the air-fuel ratio is given, and the c_p, H and ϕ are sought for the combustion gas. The changes undergone by the combustion gas are then calculated [13, 14].

The values obtained by cycle calculations are used as the calculating conditions. On the basis of hypothesis (4), the ϕ_N' defined by the following equation was assumed to be constant in the radial direction.

$$\varphi_N' = \frac{P_{t2}}{P_{t1}} \quad (2.33)$$

Furthermore, if we assume the compressor outlet temperature to be approximately 500°C, the air-fuel ratio will have to be approximately 0.015 in order for the turbine inlet temperature to be 1150°C. Therefore, calculations were performed with an air-fuel ratio of λ = 0.015. The results of these calculations, together with the sequence of calculation, are shown in Appendix Table 2. Thus, the design velocity triangle will be as shown in Fig. 2 in the main text.

The turbine adiabatic efficiency η_T as defined by the following equation was used.

$$\eta_T = \frac{\Delta H_T}{\Delta H_{ad}} \quad (2.34)$$

Here, ΔH_T and ΔH_{ad} are the actual thermal head and the adiabatic head inside the turbine from the turbine inlet total pressure to the outlet total pressure. Even though η_T = 87.4% from the results calculated in No. 61 of Table 2, the adiabatic efficiency in designing was taken at 85.0%, taking into consideration the effects of the blowout of the cooling air because the turbine is an air-cooled turbine. Consequently, the specific output ΔH_T of this turbine had a target of 53.8 kcal/kg (= $0.85 \cdot \Delta H_{ad}$).

Furthermore, the degree of reaction (ρ_R) and the theoretical velocity (V_{th}) of this turbine were defined and sought by the following equations:

$$\rho_R = \frac{H_{s2} - H_{s3}}{\Delta H_T} \quad (2.35)$$

$$V_{th} = \sqrt{2gJ \cdot \Delta H_{ad}} \quad (2.36)$$

The chief design specifications of this turbine obtained in this way are shown in Table 1 in the main text.

APPENDIX TABLE 2. SEQUENCE AND RESULTS OF CALCULATIONS OF VELOCITY TRIANGLES

CALCULATING CONDITIONS

$T_{t1}=1423.15°K$ $\alpha_2=72.0$ deg. $\varphi_N'=0.97$

$P_{t1}=25000$ kg/m² $V_{2M}=558.67$ m/sec $\lambda=0.015$

$N=13300$ r.p.m. $V_{a3,M}=232.44$ m/sec

$\Delta H_T=55.29$ kcal/kg $\pi_T=2.02$

No	Object to be calculated	Calculation equations, etc.	TIP	MEAN	ROOT	Unit
1	r	give	2.793000−01	2.633000−01	2.473000−01	m
2	r/r_M	①/r_M	1.060767+00	1.000000+00	9.392328−01	
3	U_{2M}	2π①N/60	——	3.667179+02	——	m/sec
4	$V_{2u}+V_{3u,M}$	$g\cdot J\Delta H_T$/③, Eq(2·18)	——	6.307637+02	——	m/sec
5	m	$(\sin\alpha_2)^2$	——	9.045081−01	——	
6	V_{a3}	Eq (2·26)	2.336302+02	2.324400+02	2.309665+02	m/sec
7	U	2π①N/60	3.890023−02	3.667179+02	3.444335+02	m/sec
8	V_2	V_{2M}/②^m, Eq(2.17)	5.296412+02	5.586700+02	5.912650+02	m/sec
9	V_{a2}	⑧ cos α_2	1.636685+02	1.726389+02	1.827113+02	m/sec
10	V_{2u}	⑧ sin α_2	5.037186+02	5.313266+02	5.623263+02	m/sec
11	$V_{2u}+V_{3u}$	$g\cdot J\cdot\Delta H_T$/⑦, Eq(2.18)	5.946297−02	6.307637+02	6.715733+02	m/sec
12	V_{3u}	⑪-⑯	9.091110+01	9.943708+01	1.092470+02	m/sec
13	V_3	$\sqrt{⑥^2+⑫^2}$	2.506948+02	2.528163+02	2.555004+02	m/sec
14	$V_3^2/2g\cdot J$	⑬²/2$g\cdot J$	3.352597+01	3.730169+01	4.178131+01	kcal/kg
15	H_{t1}	SUB 90 (T_{t1}, λ)	——	3.758583+02	——	kcal/kg
16	P_{t2}	$\varphi_N'\cdot P_{t1}$, Eq(2·33)	——	2.425000+04	——	kg/m²
17	H_{t2}	H_{t1}	——	3.758583+02	——	kcal/kg
18	T_{t2}	T_{t1}	——	1.423150+03	——	°K
19	H_{s2}	⑰-⑭	3.423324+02	3.385566+02	3.340770+02	kcal/kg
20	T_{s2}	SUB 90 (⑱, λ)	1.308931+03	1.295984+03	1.280599+03	°K
21	P_{s2}	SUB 100 (⑯, ㉓, ⑲, λ)	1.694543+04	1.624371+04	1.544024+04	kg/m²
22	γ_2	㉑/R⑲, Eq(2·2)	4.422961−01	4.282159−01	4.119252−01	kg/m³
23	κ_2	SUB 80 (㉑, λ)	1.307150+00	1.307751+00	1.308481+00	
24	a_2	$\sqrt{⑲gR⑳}$, Eq(2·3)	7.005601+02	6.972472+02	6.932869+02	m/cec
25	W_{2u}	⑧ sin α_2 − ②	1.147163+02	1.646087+02	2.178928+02	m/sec
26	W_2	$\sqrt{⑨^2-㉕^2}$	1.998680+02	2.385377+02	2.843602+02	m/sec
27	β_2	$\sin^{-1}$ (㉕/㉖)	3.502698+01	4.363609+01	5.001899+01	deg.
28	M_2	⑧/㉒	7.560254−01	8.012509−01	8.528398−01	
29	M_{r2}	㉖/㉒	2.852974−01	3.421135−01	4.101607−01	
30	W_{3u}	⑪-⑤	4.799134+02	4.661550+02	4.536805+02	m/sec
31	W_3	$\sqrt{⑥^2+㉚^2}$	5.337602+02	5.208923+02	5.090889+02	m/sec
32	$W_3^2/2gJ$	㉚²/2$g\cdot J$	3.404945+01	3.242752+01	3.097456+01	kcal/kg
33	H_{t3}	⑰-ΔH_T	——	3.205683+02	——	kcal/kg
34	T_{t3}	SUB 90 (㉜, λ)	——	1.234028+03	——	°K
35	P_{t3}	P_{t1}/π_T	——	1.237624+04	——	kg/m²
36	$V_3^2/2gJ$	㉝²/2$g\cdot J$	7.511185+00	7.638849+00	7.801907+00	kcal/kg
37	H_{s3}	㉞-㉜	3.130571+02	3.129295+02	3.127664+02	kcal/kg
38	T_{s3}	SUB 90 (㉟, λ)	1.208016+03	1.207573+03	1.207007+03	°K
39	P_{s3}	SUB 100 (㉟, ㉞, ㉜, λ)	1.131391+04	1.129648+04	1.127424+04	kg/m²
40	γ_3	㉜/R㉟	3.199761−01	3.196003−01	3.191207−01	kg/m³
41	κ_3	SUB 80 (㉟, λ)	1.312173+00	1.312197+00	1.312228+00	

[Continued on following page]

APPENDIX TABLE 2 (Continued)

No	Object to be calculated	Calculating equations, etc.	TIP	MEAN	ROOT	Unit
42	a_3	$\sqrt{\text{㊶}g\text{㊸}}$	6.743048+02	6.741873−02	6.740372+02	m sec
43	M_3	㊸ ㊷	8.717826−01	3.749942−01	3.790597−01	
44	M_{r3}	㊶ ㊼	7.915711−01	7.726226−01	7.552831−01	
45	β_3	$\sin^{-1}$(㊺/㊸)	6.404244+01	6.349773−01	6.301965+01	deg.
46	M_{a3}	㊹·cos㊺	3.464756−01	3.447706−01	3.426613−01	
47	α_3	$\cos^{-1}$(㊹/㊸)	2.126236+01	2.316124−01	2.531428+01	deg.
48	M_{a2}	㊻·cos α_2	2.336252−01	2.476007−01	2.635426−01	
49	$H_{s2}-H_{s3}$	㊾−㊽	2.927522+01	2.562716+01	2.131056+01	kcal kg
50	ρ_R	㊾ ΔH_T	5.294848−01	4.635045−01	3.854331−01	
51	$\bar{\kappa}$	(㊸−㊶)/2	1.309661+00	1.309974+00	1.310354+00	
52	$\bar{c}_p$	㊶R/(㊷−1)	2.899803−01	2.897575−01	2.894859−01	kcal kg·K
53	P_{t3}/P_{t1}	1. π_T	—	4.950495−01	—	
54	T_{t3}/T_{t1}	㊷ T_{t1}	—	8.671105−01	—	
55	$1-(1/\pi_T)^{(\kappa-1)/\kappa}$	㊺, ㊷	1.531597−01	1.532681−01	1.534001−01	
56	η_t	ΔH_T/㊷ T_{t1}㊷	8.747481−01	8.748026−01	8.748689−01	
57	η_{t-s}	(1−㊻)/㊺	8.676531−01	8.670391−01	8.662934−01	
58	T_{t2ad}	SUB 110 (T_{t1}, π_T, λ)	—	1.206500+03	—	K
59	H_{t2ad}	SUB 90 (㊺, λ)	—	3.126040+02	—	kcal kg
60	ΔH_{ad}	㊾−㊽	—	6.325431+01	—	kcal kg
61	η_T	ΔH_T/㊿, Eq(2·34)	—	8.740906−01	—	

Reference: Concerning the subroutines used

SUBOUTINE	INPUT	OUTPUT	Reference
SUB 80	T, λ	κ, c_p	(13, 14)
〃 90	T(or H), λ	H(or T)	
〃 100	P_1, T_1, T_2, λ	P_2	
〃 110	P_{t1}, P_{t1}/P_{t2}, λ	T_{t2}	

3. Determining the Profile and Arrangement of the Air-Cooled Blades

(a) Stator Blades

We used the method of basing ourselves on the camber line and of "fleshing it out" suitably. That is, here we approximated the camber line by a cubic expression; we drew a series of circles having their centers on the curve; and we assumed that their envelopes were the external shape of the blade. In the

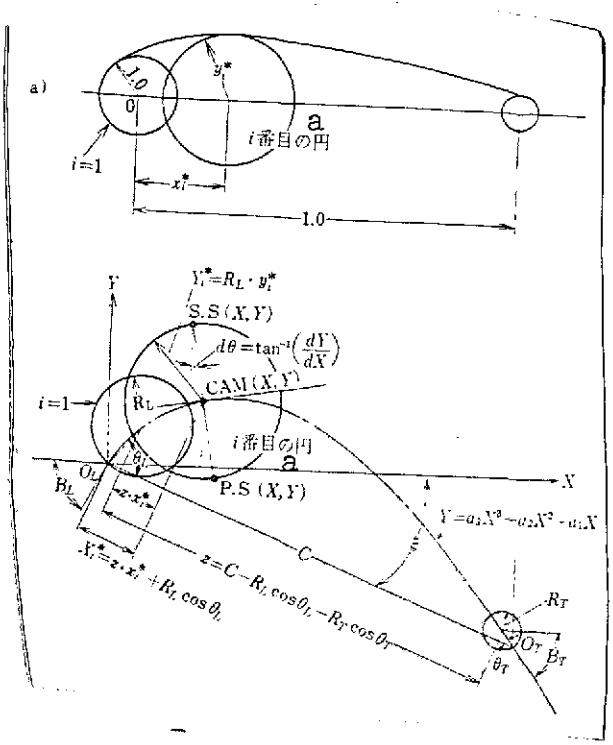

Appendix Fig. 1. Method of calculating stator blade profile and blade arrangements.

Key: a. i-th circle

following, this method is described in detail (see Appendix Fig. 1).

(1) Determining the camber line: We took the blade's leading edge O_L as the point of origin, /27 as in Appendix Fig. 1 (b). Then we plotted coordinate systems with the axial direction as the X axis and the circumferential direction as the Y axis. The camber line was expressed by the following cubic expression

$$Y=a_3X^3+a_2X^2+a_1X$$

The angles formed by the tangents on this camber line at the blade leading edge O_L and trailing edge O_T with the X-axis direction are defined as the blade inlet angle B_L and the outlet angle B_T, respectively. The angle formed by the chord connecting O_L and O_T with the X-axis direction is defined as the angle of stagger ξ, and the length of the chord is defined as the chord length C.

If B_L, B_T, ξ, and C are assigned suitably with due consideration to the fundamental policies (1), (3), and (4), it is possible to determine the coefficients a_1, a_2, and a_3 of the cubic expression.

(2) Method of "fleshing out": When the shape of the camber line has been determined, the points on it CAM (X,Y) can be

represented by coordinate X* on the blade chord (orthogonal projection of point CAM(X,Y) on the blade chord). Next there is a shift from this coordinate to a new coordinate system x* (Appendix Fig. 1 (a)) which has been made dimensionless so that the center of the circle i = 1 (circle corresponding to the blade leading edge) will correspond to x* = 0 and the center of the circle i = m (circle corresponding to the blade trailing edge) will correspond to x* = 1. In Appendix Fig. 1 (b), the distance between the X* coordinates centering in circle i = 1 and i = m will be:

$$z = C - R_L \cos\theta_L - R_T \cos\theta_T$$

Therefore, this will be the divisor for conversion to dimensionless terms in shifting from X* to x*. Here, θ_L is the angle between the blade chord and the line connecting the center of the circle i = 1 and O_L. θ_T is the angle between the blade chord and the line connecting the center of i = m and O_T.

Thus, the correspondence between x* and the coordinate CAM(X,Y) on the camber line will be valid. On the other hand, if we divide the radius Y* of the circle determining the blade thickness at CAM(X,Y) by the blade leading edge radius R_L (Y* of the circle i = 1) to render it dimensionless and represent it as y*, then plot a circle with a radius y* at point x*, the results will be as shown in Appendix Fig. 1 (a). This will form a symmetrical blade profile, and the blade thickness will be given in this shape so that there will be a good shape from the aerodynamical standpoint.

On the contrary, if we supply the blade thickness distribution on the (x*,y*) plane as shown in Appendix Fig. 1 (a) and also supply the blade leading edge radius according to fundamental policy (3), the blade trailing edge radius R_T will be determined from the ratio between the radius y* of the circle

i = m and R_L. Furthermore, θ_L and θ_T will be determined if we use a known camber line equation. Therefore, z can be calculated from the equation given above. Consequently, with respect to a certain x_i^* in Appendix Fig. 1 (a), one performs conversion

$$X_i^* = z x_i^* + R_L \cos\theta_L$$

The position X_i^* on the blade chord on the physical plane in Appendix Fig. 1 (b) will thus be determined, and the coordinate CAM(X,Y) on the camber line will also be determined. On the other hand, the blade thickness Y_i^* will also be determined using the relationship

$$Y_i^* = R_L \cdot y_i^*$$

on the basis of the relationship of y_i^* to x_i^* in Appendix Fig. 1 (a). In the final analysis, if one draws a circle with a radius Y_i^* centering around point CAM(X,Y) in Appendix Fig. 1 (b) and finds the two points of intersection between it and the normal lines established on the camber line at this point, they will be the coordinates on the upper and lower surfaces of the blade, S.S(X,Y) and P.S(X,Y).

(3) Since the blade profile has been determined by the above, the blade arrangement can next be determined if the number of blades n is given. Therefore, the pitch S and the throad width O will be determined, and $\cos^{-1}(O/S)$ can be calculated.

In this manner, the blade profiles and blade arrangements were calculated by means of a computer for several values of B_L, B_T, ξ, C, R_L, and n, and the blades to be adopted were determined in accordance with fundamental policies (1) and (2). That is, taking into consideration the influence of the Mach number and the curvature of the rear blade surface from the throat part to the trailing edge, we adopted a design in which the calculated

value of $\cos^{-1}(O/S)$, mentioned above, would be slightly smaller than the stator blade absolute outflow angle (α_2) of 72.0° of the design velocity triangle [15], and in which the number of blades would be as small as possible.

As for the blade thickness distribution, the blade thicknesses of air-cooled blades [2] having a design velocity triangle relatively similar to theseaair-cooled blades were calculated in reverse and used in the form shown in Appendix Fig. 1 (a). They are shown in Appendix Table 3. The same blade thickness distribution was used in every section, the TIP, the MEAN, and the ROOT (the chord length was different)

APPENDIX TABLE 3. BLADE THICKNESS DISTRIBUTION USED IN CALCULATING STATOR BLADE PROFILES [2]

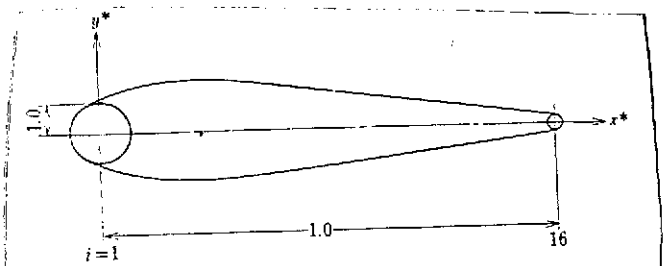

i	x^*	y^*	i	x^*	y^*
1	0.000	1.000	9	0.398	1.362
2	0.032	1.289	10	0.474	1.171
3	0.069	1.447	11	0.550	1.026
4	0.108	1.513	12	0.633	0.901
5	0.153	1.631	13	0.719	0.763
6	0.202	1.658	14	0.810	0.605
7	0.264	1.572	15	0.907	0.428
8	0.329	1.461	16	1.000	0.237

(b) Rotor Blades

Several blade profiles and blade arrangements were determined for the TIP, the MEAN, and the ROOT following the fundamental policies, and the blade surface velocities were sought experimentally for each by the electrical analog method using electroconductive paper [16]. The blade loss and blade inlet critical Mach number were estimated from the results, and we adopted the design which had the smallest blade loss and in which the blade inlet critical Mach number had an adequate margin and was considerably larger than the design inlet Mach number of the rotor blades. In the following this method is described in stages.

(1) Following fundamental policy (1), the solidity giving the least profile loss (optimum solidity) was determined by means of entry [15] in the bibliography, taking into consideration the rotor blade outflow angle and the degree of reaction for each section. It was determined so that the solidity would be slightly smaller than the optimum solidity because of fundamental policy (2), considering the fact that the blades are air-cooled blades.

(2) Next, following fundamental policy (4), it was assumed that there are almost no changes of the chord length in the blade span direction, and the chord length and number of blades were determined, taking into consideration the solidity determined in (1), so that the aspect ratio would not be too small.

(3) The blade leading edge and trailing edge diameters were determined in accordance with fundamental policy (3).

(4) On the other hand, the throat width O was determined from the rotor blade relative outflow angle β_3 in the velocity triangle. In other words, the difference between β_3 and $\cos^{-1}(O/S)$ was determined by means of entry [15] in the bibliography, taking into consideration the influence of the design outflow Mach number. /28

(5) Next, the incidence at the design point was determined slightly on the minus side from the zero incidence, taking into consideration the operating range of the turbine. This decision was made on account of the general tendency of the characteristic curves of the profile loss so that the efficiency would not drop even at partial loads. The inlet angle of the blades B_L was determined from this incidence and from the β_2 of the velocity triangle.

(6) Next, the angle of stagger was determined, and a blade profile was drawn so as to satisfy the previously determined pitch S, the leading edge diameter d_L, the trailing edge diameter d_T, the throat width O, and the blade inlet angle B_L. At this time, the curvature of the back surface of the blade between the throat part and the trailing edge will have an influence on the outflow angle. Therefore, this was taken into consideration when making the decision [15]. Since there is still a certain degree of freedom in the blade profile and blade arrangements even under these conditions, several blade profiles were drawn. The designs for the rotor blades, unlike those for the stator blades, were drawn manually without using a computer.

(7) In this way, three types of blade profiles and blade arrangements were compiled for the TIP, the MEAN, and the ROOT, making up a total of nine designs. Since the goal was to select blades which would have the optimum pressure distribution and which would also have a low heat transfer rate outside the blades, in accordance with fundamental policy (5), the surface velocity distribution was sought by the electrical analog method for each of the blades. The following equations were used to calculate blade diffusion parameters (D) from these results. /29

$$\left.\begin{aligned} D_s &= 1-\frac{V_2}{V_s} \\ D_p &= 1-\frac{V_p}{V_1} \\ D_t &= D_p+D_s \end{aligned}\right\} \qquad (3.1)$$

Here, V_L is the blade inlet velocity, V_2 is the blade outlet velocity, V_s is the maximum surface velocity on the back surface of the blade, and V_p is the maximum surface velocity on the belly surface of the blade. According to entry [17] in the bibliography, the specific blade loss L ($L = (1 - \eta_t)/\sigma_N$ [sic]; here η_t is the adiabatic efficiency calculated from the turbine output, and σ_M [sic] is the solidity at the MEAN) is particularly influenced by D_s but generally declines together with the decline of D_t. Therefore, we selected the design with the smallest D_s and D_t. The results of the surface velocity distribution of the rotor blades adopted in this turbine are shown in Appendix Fig. 2, and the results of calculations of the D_s, D_p, and D_t are shown in Appendix Table 4.

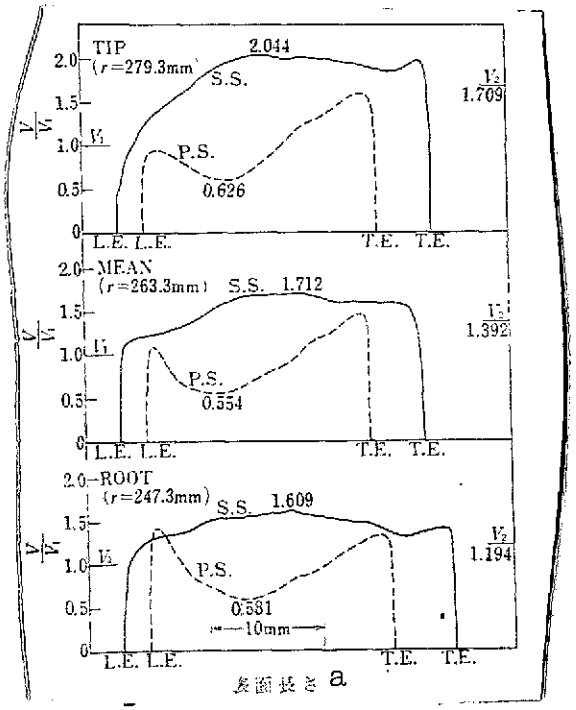

Appendix Fig. 2. Rotor blade surface velocity distribution by electrical analog method.

Key: a. Surface length

The maximum pressure coefficient on the back surface of the blade $C_{pi,max}$ was sought from the results in Fig. 5 by means of

$$C_{pi,max} = 1 - \left(\frac{V_s}{V_1}\right)^2 \qquad (3.2)$$

The pressure coefficient influencing the compressibility and the critical inflow Mach number at the blade inlet were determined using the Karman-Tsien method [18, 19]. That is, according to the Karman-Tsien method, the relationship between the pressure coefficient C_p considering the compressibility and the pressure coefficient of an incompressible fluid C_{pi} is expressed as follows:

APPENDIX TABLE 4. VALUES OF ROTOR BLADE DIFFUSION PARAMETERS, PRESSURE COEFFICIENTS, AND CRITICAL INFLOW MACH NUMBERS

	TIP (r=277.3mm)	MEAN (r=261.3mm)	ROOT (r=245.3mm)
D_s	0.164	0.187	0.258
at (d/c)	(0.240)	(0.251)	(0.267)
D_p	0.374	0.446	0.419
D_t	0.538	0.633	0.677
$C_{pi,\max}$	−3.178	−1.931	−1.589
$C_{p,\max}$	−4.0	−2.4	−2.1
$M_{1,cr}$	0.39	0.48	0.51

$$C_p=\frac{C_{pi}}{\sqrt{1-M_\infty^2}+\frac{M_\infty^2}{1+\sqrt{1-M_\infty^2}}\cdot\frac{C_{pi}}{2}} \qquad (3.3)$$

Furthermore, in view of the definition of the pressure coefficient C_p,

$$C_p=\frac{2}{\kappa M_\infty^2}\left\{\left(\frac{1+\frac{\kappa-1}{2}M_\infty^2}{1+\frac{\kappa-1}{2}M^2}\right)^{\frac{\kappa}{\kappa-1}}-1\right\} \qquad (3.4)$$

Here, M_∞ is the mainstream Mach number at an infinite distance, and M is the local Mach number on the blade surface. If we use $C_{pi,max}$, $C_{p,max}$, and $M_{\infty,cr}$ to represent the C_{pi}, C_p and M_∞ when M = 1.0, their relationships will be as shown in Appendix Fig. 3, using equations (3.3) and (3.4). Let us assume that the Mach number M_1 of the mainstream at the blade inlet is identical with the M_∞ in the Karman-Tsien equation. Then we can seek the critical inflow Mach number $M_{1,cr}$ (= $M_{\infty,cr}$) at the blade inlet and the maximum pressure coefficient of the blade taking into consideration the compressibility $C_{p,max}$ for the TIP, MEAN, and ROOT sections from the values of $C_{pi,max}$ sought previously from equation (3.2) and from Appendix Fig. 3. These results are shown in

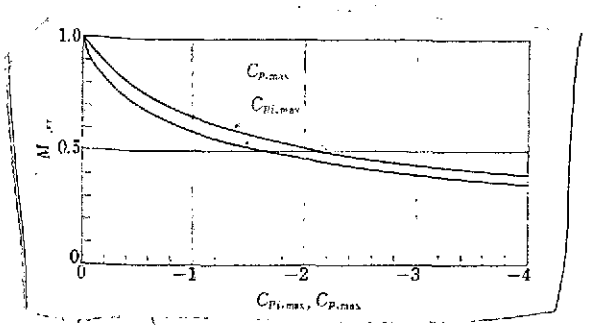

Appendix Fig. 3. Relationship between maximum pressure coefficient and critical Mach number (κ = 1.315).

Appendix Table 4. As a result, it was possible to ascertain that the blade inlet critical Mach number $M_{1,cr}$ is considerably greater than the rotor blade inlet Mach number M_{r2} in the design velocity triangle, and that the blade profile and blade arrangements were satisfactory.

(8) Finally, some modifications were incorporated so that the blade shapes would be smooth together with the stacking of the blade profiles having different sections sought in accordance with fundamental policyy (4). On account of this, the throat width O was finally aligned at the MEAN, while it was slightly smaller at the TIP and slightly larger at the ROOT. Consequently, the condition in the design policty that the work distribution in the rotor blades must be constant in the radial direction (hypothesis (7) in Section 2.2 of the main text) was not completely satisfied, there being excessive work at the TIP and insufficient work at the ROOT, while the design specifications were satisfied at the MEAN.

APPENDIX B. EQUIVALENT CONDITIONS OF TURBINE OPERATING STATES [20-22]

(a) Hypotheses

The equivalent conditions of the turbine operating states are sought under the following hypotheses.

1) It is assumed that, when the Mach number M of the flow inside the blade and the Mach number M_u of the peripheral velocity are identical, the flow will be similar. The similarity conditions are to be determined while ignoring the effects of the Reynolds' number.

2) The fluid inside the turbine is assumed to be a perfect gas, and the flow is assumed to be an adiabatic single-dimensional flow. /30

3) The specific heat ratio inside the turbine is assumed to be constant.

(b) Fundamental Equations

Equation for the relationship between the total temperature and the static temperature:

$$\frac{T_t}{T_s}=1+\frac{\kappa-1}{2}M^2 \tag{4.1}$$

Equation for the relationship between the total pressure and the static pressure:

$$\frac{P_t}{P_s}=\left(1+\frac{\kappa-1}{2}M^2\right)^{\frac{\kappa}{\kappa-1}} \tag{4.2}$$

Equation for the perfect gas:

$$\gamma=\frac{P_s}{R\cdot T_s} \tag{4.3}$$

Equation for the relationship between the velocity and the Mach number:

$$V=M\sqrt{\kappa\cdot g\cdot R\cdot T_s} \tag{4.4}$$

Equation for the flow rate: Assuming that the flow is a single-dimensional flow:

$$G=\gamma\cdot A\cdot V \tag{4.5}$$

(c) Derivation of the Equivalent Conditions

Corrected Flow Rate

The following equation is obtained by using equations (4.1)-(4.4) in the continuous equation (4.5).

$$M^2=\frac{G\cdot V}{P_t}\cdot\frac{\left(1+\frac{\kappa-1}{2}M^2\right)^{\frac{\kappa}{\kappa-1}}}{\kappa}\frac{1}{A\cdot g}$$

The above equation is valid also at the standard state. In other words, it can be written in the following manner if the subscript st is used to indicate the standard state.

$$M_{st}^2=\frac{G_{st}\cdot V_{st}}{P_{t,st}}\cdot\frac{\left(1+\frac{\kappa_{st}-1}{1}M_{st}^2\right)^{\frac{\kappa_{st}}{\kappa_{st}-1}}}{\kappa_{st}}\frac{1}{A\cdot g}$$

If we assume that the flow is similar to the flow at the standard state, because M = M_{st}, the flow rate at the standard state G_{st} can

can be expressed in the following terms on account of the two equations given above

$$G_{st}=\frac{\varepsilon\cdot G\cdot\sqrt{\theta}}{\delta}$$

Here,

$$\theta=\left(\frac{V}{V_{st}}\right)^2=\frac{\left(\frac{\kappa\cdot T_t}{1+\frac{\kappa-1}{2}M^2}\cdot R\right)}{\left(\frac{\kappa_{st}\cdot T_{t,st}}{1+\frac{\kappa_{st}-1}{2}M^2}\cdot R_{st}\right)}$$

$$\delta=\frac{P_t}{P_{t,st}} \qquad (4.6)$$

$$\varepsilon=\frac{\kappa_{st}}{\kappa}\cdot\frac{\left(1+\frac{\kappa-1}{2}M^2\right)^{\frac{\kappa}{\kappa-1}}}{\left(1+\frac{\kappa_{st}-1}{2}M^2\right)^{\frac{\kappa_{st}}{\kappa_{st}-1}}}$$

In other words, when the flow rate at a certain state is G, the flow rate at the standard state, where the flow is similar with that state, can be written as $\varepsilon\cdot G\cdot\sqrt{\theta}/\sigma$. Because of this, the equivalent conditions of the flow rate are that $\varepsilon\cdot G\cdot\sqrt{\theta}/\sigma$ is identical.

Corrected Revolution Speed

The relationship between the revolution speed and the peripheral velocity is expressed by the following equation

$$U=\frac{\pi\cdot D\cdot N_{st}}{60} \qquad (4.7)$$

Here, D is the diameter of revolution and N is the revolutions per minute. If we use equation (4.4) to express the peripheral velocity in terms of the Mach numbers, since $M_u = U/\sqrt{\kappa\cdot g\cdot R\cdot T_s}$, the following will be obtained from equation (4.7)

$$M_u = \frac{\pi \cdot D \cdot N}{60} \cdot \frac{M}{V}$$

This equation will be equally valid in the standard state as well.

$$M_{u,st} = \frac{\pi \cdot D \cdot N_{st}}{60} \cdot \frac{M_{st}}{V_{st}}$$

If we assume that the flow is similar to the flow in the standard state, since M = M_{st} and $M_u = M_{u,st}$, the revolution speed at the standard state N_{st} can be expressed as follows on the basis of the two preceding equations.

$$N_{st} = \frac{N}{\left(\frac{V}{V_{st}}\right)} = \frac{N}{\sqrt{\theta}} \qquad (4.8)$$

Consequently, the equivalent conditions for the revolution speed are that $N/\sqrt{\theta}$ is identical.

Corrected Specific Output

The enthalpy drop is expressed by the following equation

$$\Delta H = \frac{V^2}{2 \cdot g \cdot J} \qquad (4.9)$$

This equation is valid similarly also at the standard state.

$$\Delta H_{st} = \frac{V_{st}^2}{2 \cdot g \cdot J}$$

If we assume that the flow is similar to the flow at the standard state, since M = M_{st}, the enthalpy drop at the standard state ΔH_{st} can be expressed as follows on the basis of the two preceding equations.

$$\Delta H_{st}=\frac{\Delta H}{\left(\frac{V}{V_{st}}\right)}=\frac{\Delta H}{\theta} \qquad (4.10)$$

Consequently, the equivalent conditions for the enthalpy drop (specific output) are that $\Delta H/\theta$ is identical.

Corrected Torque

The torque τ is expressed by the following equation using the flow rate G, the revolution speed N, and the specific output ΔH.

$$\tau=\frac{60\cdot J}{2\pi}\cdot\frac{G\cdot\Delta H}{N} \qquad (4.11)$$

/31

The above equation is valid also at the standard state.

$$\tau_{st}=\frac{60\cdot J}{2\pi}\cdot\frac{G_{st}\cdot\Delta H_{st}}{N_{st}}$$

If we substitute equations (4.6), (4.8), and (4.10) in this equation, we obtain:

$$\tau_{st}=\frac{60\cdot J}{2\pi}\cdot\frac{\varepsilon\cdot G\cdot\sqrt{\theta}}{\delta}\cdot\frac{\Delta H}{\theta}=\frac{\varepsilon}{\delta}\left(\frac{60\cdot J}{2\pi}\cdot\frac{G\cdot\Delta H}{N}\right) \qquad (4.12)$$

Furthermore, if we use equation (4.11), the torque at the standard state τ_{st} can be written as follows.

$$\tau_{st}=\frac{\varepsilon\cdot\tau}{\delta} \qquad (4.13)$$

Consequently, the equivalent conditions of the torque are that $\varepsilon\cdot\tau/\delta$ is identical.

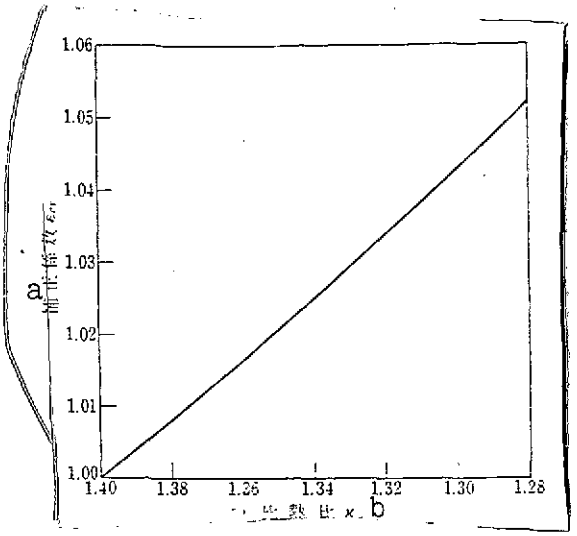

Appendix Fig. 4. Flow rate correction coefficient.

Key: a. Correction coefficient; b. Specific heat ratio

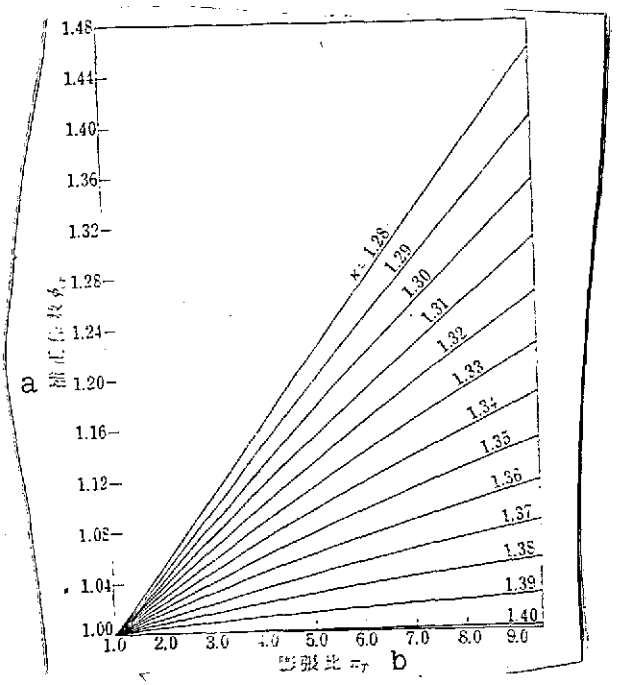

Appendix Fig. 5. Expansion ratio correction coefficient.

Key: a. Correction coefficient; b. Expansion ratio

Corrected Expansion Ratio

The adiabatic efficient η_t of the turbine is defined by the following equation

$$\eta_t=\frac{\Delta H}{\frac{\kappa}{\kappa-1}\cdot\frac{R}{J}\cdot T_{t1}\left[1-\left(\frac{1}{\pi_T}\right)^{\frac{\kappa-1}{\kappa}}\right]} \qquad (4.14)$$

The equation is also valid at the standard state.

$$\eta_{t,st}=\frac{\Delta H_{st}}{\frac{\kappa_{st}}{\kappa_{st}-1}\cdot\frac{R_{st}}{J}\cdot T_{t,st}\left[1-\left(\frac{1}{\pi_{T,st}}\right)^{\frac{\kappa_{st}-1}{\kappa_{st}}}\right]}$$

If we assume that $\eta_t = \eta_{t,st}$ when the flow is similar to the flow at the standard state, the following can be obtained from the two preceding equations.

$$\frac{1-\left(\frac{1}{\pi_{T,st}}\right)^{\frac{\kappa_{st}-1}{\kappa_{st}}}}{1-\left(\frac{1}{\pi_T}\right)^{\frac{\kappa-1}{\kappa}}}=\left(\frac{\kappa_{st}-1}{\kappa-1}\right)\left(\frac{\kappa\cdot R\cdot T_{t1}}{\kappa_{st}\cdot R_{st}\cdot T_{t,st}}\right)\frac{\Delta H_{st}}{\Delta H}$$

Furthermore, if we transform it using equations (4.6) and (4.10), we obtain:

$$\frac{1-\left(\frac{1}{\pi_{T,st}}\right)^{\frac{\kappa_{st}-1}{\kappa_{st}}}}{1-\left(\frac{1}{\pi_T}\right)^{\frac{\kappa-1}{\kappa}}}=\left(\frac{\kappa_{st}-1}{\kappa-1}\right)\frac{1+\frac{\kappa-1}{2}M^2}{1+\frac{\kappa_{st}-1}{2}M^2}$$

From this, when we solve for the expansion ratio at the standard state $\pi_{T,st}$, the following equation is obtained:

$$\pi_{T,st}=\phi\cdot\pi_T$$

Here,

$$\phi=\frac{1}{\pi_T}\left\{1-\left(\frac{\kappa_{st}-1}{\kappa-1}\right)\left(\frac{1+\frac{\kappa-1}{2}M^2}{1+\frac{\kappa_{st}-1}{2}M^2}\right)\left(1-\pi_T^{\frac{1-\varepsilon}{\varepsilon}}\right)\right\}^{\frac{\kappa_{st}}{1-\kappa_{st}}} \tag{4.15}$$

Consequently, the equivalent conditions of the expansion ratio are that $\phi\cdot\pi_T$ is identical.

(d) Approximate Treatment of the Various Equivalent Condition Equations

As was mentioned above, the equations for the equivalent conditions for the flow rate, the revolution speed, the specific output, the torque, and the expansion ratio can be expressed in terms of equations (4.6), (4.8), (4.10), (4.13), and (4.15), respectively. Since the flow inside the turbine is usually close to Mach 1, if we assume that M is approximately equal to 1.0 in these equations, the equations for θ, ε and ϕ containing M will be as follows. Let us use the subscript cr to indicate the values of θ, ε and ϕ when M = 1.0. In this case, θ will be as follows on the basis of equation (4.6): /32

$$\theta_{cr}=\left(\frac{V_{cr}}{V_{cr,st}}\right)^2=\frac{\frac{\kappa}{\kappa+1}\cdot R\cdot T_t}{\frac{\kappa_{st}}{\kappa_{st}+1}\cdot R_{st}\cdot T_{t,st}} \tag{4.16}$$

ε will also be as follows on the basis of equation (4.6):

$$\varepsilon_{cr}=\frac{\kappa_{st}}{\kappa}\frac{\left(\frac{\kappa+1}{2}\right)^{\frac{\kappa}{\kappa-1}}}{\left(\frac{\kappa_{st}+1}{2}\right)^{\frac{\kappa_{st}}{\kappa_{st}-1}}}$$

また，ϕ は式 (4.15) より，

$$\phi_{cr}=\frac{1}{\pi_T}\left\{1-\left(\frac{\kappa_{st}-1}{\kappa-1}\right)\left(\frac{\kappa+1}{\kappa_{st}+1}\right)\right. \qquad (4.17)$$

ϕ will be as follows on the basis of equation (4.15):

$$\left.\times\left(1-\pi_T^{\frac{1-\kappa}{\kappa}}\right)\right\}^{\frac{\kappa_{st}}{1-\kappa_{st}}} \qquad (4.18)$$

There θ_{cr}, ε_{cr} and ϕ_{cr} may be used approximately in the aforementioned equivalent condition equations.

In this report, the following values were adopted for the standard state:

$T_{t,st}=288.2\,^{\circ}\mathrm{K}$
$P_{t,st}=10332\,\mathrm{kg/m^2}$
$R_{st}=29.27\,\mathrm{kg\cdot m/^{\circ}K\cdot kg}$
$\kappa_{st}=1.401$

In this case, ε_{cr} and ϕ_{cr} may be depicted graphically in terms of the differences in the specific heat ratio. They will be as shown in Appendix Figs. 4 and 5. It is clear that, when the specific heat ratio differs considerably from the standard state, ε_{cr} and ϕ_{cr} will have magnitudes great enought to require consideration.